

THESIS

DEVELOPMENT OF A HALL THRUSTER TEST FACILITY

Submitted by

Randolph W. Leach

Department of Mechanical Engineering

In partial fulfillment of the requirements

For the Degree of Master of Science

Colorado State University

Fort Collins, Colorado

Fall 2012

Master's Committee:

Advisor: Azer P. Yalin

John D. Williams
Carmen S. Menoni

Copyright by Randolph W. Leach 2012

All Rights Reserved

ABSTRACT

DEVELOPMENT OF A HALL THRUSTER TEST FACILITY

The present thesis details the development of a Hall thruster test facility for low power ($\lesssim 600$ W) thrusters. The facility is based on a vacuum chamber, two standard cryogenic pumps and one modified cryogenic pump. The modified cryogenic pump is outfitted with custom built internal components, which are referred to as a cryosail. Estimation as well as measurement of pumping speeds of the two cryogenic pumps and cryosail were conducted resulting in an overall measured pumping speed of 10,500 L/s for Xenon. The ultimate base pressure of the system was 4×10^{-8} Torr. A SPT-70 Hall thruster was operated at various conditions and set points to include fine tuning the current to the magnets to find efficient thruster operation. Ion current densities at points downstream of the thruster's exit plane were examined by a Faraday probe. Although operation at nominal thruster operating conditions was not achieved, likely due to a problem with magnetic coils, the thruster operation did allow preliminary measurements by Cavity Ring-Down Spectroscopy of sputtered Boron originating from the thruster channel wall.

DEDICATION

This thesis is dedicated to all the brave women and men of our Armed Forces. For the following Marine and Soldiers that I had the privilege and honor to know and serve with but who did not make it home, you will never be forgotten...

2nd Lt John T. Wroblewski
CW2 Johnny V. Mata
1SG Timmy J. Millsap
SSG Sean G. Landrus
SSG Oscar D. Medina
SPC Ramon C. Ojeda

TABLE OF CONTENTS

ABSTRACT.....	ii
DEDICATION.....	iii
LIST OF KEYWORDS	vi
LIST OF SYMBOLS	vii
1.0 INTRODUCTION – HALL THRUSTER PROPULSION	1
1.1. Principles of Operation	2
1.2. Governing Equations	5
1.3. Propulsion Characteristics	7
1.4. History and Development	8
1.5. Thruster Channel Material Properties.....	10
1.6. Sputter Erosion in Hall Thrusters	11
1.6.1. Mechanisms of Physical Sputtering.....	11
1.7. Problem Statement.....	14
1.8. Thesis Layout.....	16
2.0 DEVELOPMENT OF THE HTECh.....	17
2.1. Components and Design	17
2.2. Cryogenic Pumps	23
2.3. Cryosail Construction	26
2.4. Estimated Pumping Speeds.....	28
2.4.1. CT 10 and CT 500 Pumping Speed Calculations	29
2.4.2. Cryosail Pumping Speed Calculation	29
2.4.3. Summary of Estimated Pumping Speed Calculations	30
2.5. Pumping Speed Test Results.....	31
2.6. Comparison of Estimated to Measured Pumping Speeds.....	34
2.7. HTECh Conditions versus Space Conditions	34
3.0 INTIAL TESTING OF A SPT-70 HALL THRUSTER.....	36
3.1. Installation and Supporting Equipment	37
3.2. Expected Operating Conditions	39
3.3. SPT-70 Operation	40

3.4.	Faraday Probe Measurements	43
3.5.	Thruster Operation Issues	47
4.0	SPUTTER EROSION STUDY BY CRDS.....	49
4.1.	CRDS Technique Overview	49
4.2.	Preliminary CRDS Results	51
5.0	CONCLUSION.....	54
6.0	REFERENCES	58
	APPENDIX A – CATHODE START-UP PROCEDURE.....	62
	APPENDIX B – SYSTEM WIRING DIAGRAM AND THRUSTER START-UP PROCEDURE	64

LIST OF KEYWORDS

AEHF – Advanced Extremely High Frequency
AFRL – Air Force Research Lab
Ar - Argon
BN – Boron Nitride
BN-SiO₂ - Borosil
CRDS – Cavity Ring-Down Spectroscopy
CSU – Colorado State University
CT – Cryo-Torr®
DC – direct current
H – Hydrogen
He – Helium
HTECh – Hall Thruster Erosion Chamber
HTPS – Hall Thruster Propulsion System
Kr - Krypton
LADS – Large Area Deposition System
LIF - Laser Induced Fluorescents
LPDL – Laser and Plasma Diagnostics Lab
N / N₂ – Nitrogen
Ne – Neon
O / O₂ – Oxygen
PPT – Pulsed-Plasma Thrusters
SPT – Stationary Plasma Thruster
TAL – Thruster with Anode Layer
VF-5 – Vacuum Facility 5 at NASA Glenn Research Center
Xe – Xenon

LIST OF SYMBOLS

A – Ampere, measure of current

amu – atomic mass unit

atoms/ion – a measure of sputter yield

C – coulomb

cm – centimeter

°C – degrees Celsius, a measure of temperature

eV – electron volt, a unit of energy equal to approximately 1.6×10^{-19} joule; also described as the amount of energy gained by the charge of a single electron moved across an electric potential difference of one volt

°F – degrees Fahrenheit, a measure of temperature

G – Gauss, a measure of magnetic induction

K – Kelvin, a measure of temperature

km/s – kilometers per second, a measure of speed

mm³/C – a measure of sputter yield

mN – millinewton, unit of force equal to 10^{-3} N

N – Newton, units of force

nm –nanometer

psi – pounds per square inch, a measure of pressure

sccm – standard (atmosphere) cubic centimeters per minute, a measure of mass flow rate

W – Watt

V – Volt, measure of electric potential

1.0 INTRODUCTION – HALL THRUSTER PROPULSION

This thesis details the development of a vacuum chamber for the purpose of testing an electric propulsion thruster. Specifically, the estimated and measured characteristics of a purpose-built vacuum chamber are presented as well as Hall thruster probe diagnostics and initial measurement results. Typical electric propulsion testing facilities are comprised of large chambers (~2 – 20 meters in length and ~1 –10 meters in diameter) with vacuum pumps capable of sustaining high gas removal rates (~50,000 – 1,600,000 L/s) and creating low pressures thus simulating space conditions. The purpose of this research effort is to assemble a relatively small chamber capable of creating and maintaining the vacuum conditions typically used for performance measurements of low power ($\lesssim 600$ W) Hall thrusters. The small vacuum chamber with associated equipment commissioned specifically to test a SPT-70 Hall thruster is referred to as the Hall Thruster Erosion Chamber (HTECh). Additionally, this effort included the development of diagnostic tools to characterize the plume of the thruster. Measurements included current density profiles of the plume and sputtered Boron from the thruster channel walls.

Hall thrusters are used for propulsion of spacecraft such as communication satellites and space exploration vehicles. The primary life limiting component in Hall thrusters is the channel wall material [1]. The channel walls are typically made from a ceramic material such as Boron Nitride (BN) or Borosil (BN-SiO₂) [2], [3]. After repeated thruster firing or continuous operation, the wall material thins due to ion sputtering and eventually wears through exposing the underlying electric and magnetic components causing the thruster to cease operation. Additionally, sputtered material can contaminate spacecraft surfaces, which may affect spacecraft operation. Large vacuum chambers with high pumping speeds capable of testing

larger Hall thrusters are typical only found in facilities operated by organizations such as NASA. For example, the NASA Glenn Research Center has a 4.5 m diameter by 18 m long vacuum chamber referred to as Vacuum Facility 5 (VF-5). VF-5 uses 40 m² of cryopanelled cooled to 20 K by a closed loop Helium (He) refrigeration system to provide high vacuum. VF-5 is capable of a pumping speed of 1.6x10⁶ L/s of Xenon (Xe) [4]. Large vacuum chambers such as VF-5 are resource intensive, expensive and require a team of engineers and scientists to operate. However, smaller Hall thrusters such as the SPT-70 can be tested and produce accurate performance measurements in much smaller vacuum chambers because pumping speed requirements are much less for smaller thrusters owing to their smaller propellant flow rates [5].

1.1. Principles of Operation

Hall thrusters, also known as Hall effect thrusters, rely on the Hall effect to confine electrons and accelerate ions to produce thrust [6]. Hall thrusters are divided into two types, the Stationary Plasma Thruster (SPT) and the Thruster with Anode Layer (TAL). The two types of thrusters are similar in layout and operating principles, however, their discharge chamber walls are significantly different. In the SPT, the chamber walls are made of an electrically insulating material used to protect the underlying magnetic poles from plasma erosion. In the TAL, the chamber walls are made of an electrically conductive material and ion acceleration occurs in a thin layer that is very close to the anode, hence its name. The short discharge chamber allows the majority of its plasma to be located downstream of its exit plane and therefore erosion protection of the magnetic poles is not needed [7]. Due to better performance and ease of operation, SPT thrusters are much more common for use on spacecraft. Consequently, investigation of the SPT Hall thruster chamber wall erosion problem is the focus of this thesis and the test facility development.

Hall thrusters are comprised of four major components as illustrated in Figure 1.1. The first major component is the anode, which is typically integrated with the thruster's propellant gas distribution scheme. The anode is biased positive and the electrons orbiting the core of the

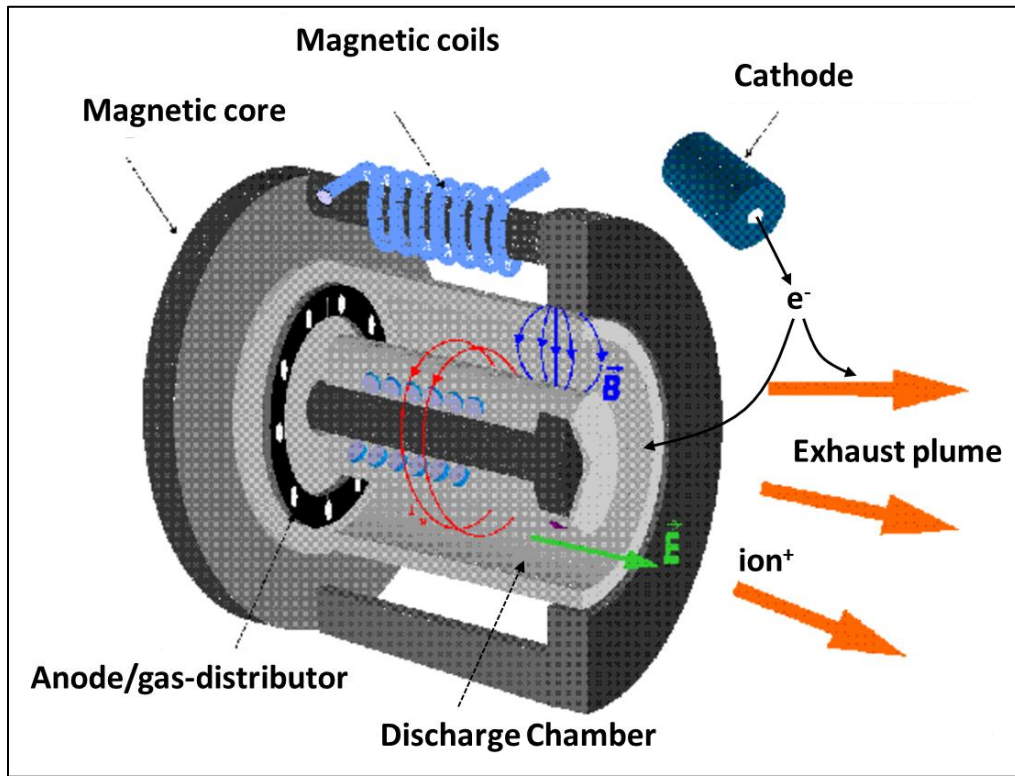


Figure 1.1. Hall Thruster schematic showing typical major components [8].

thruster (denoted by the red lines in Figure 1.1) make several revolutions around the core before being collected by the anode. During these revolutions, electrons collide with the neutral atoms from the propellant gas creating ions and secondary electrons. The resulting matter is collectively known as plasma. The voltage applied to the anode, used for both ionization and acceleration, is referred to as the discharge voltage [9].

The second major component is the magnets located symmetrically around the thruster. The magnets create a radial magnetic field that confines the electrons as they move toward the anode. The four outer magnets and one inner magnet concentrate the radial magnetic field such

that it is strongest in the vicinity of the thruster exit [10]. The magnetic field is chosen to be strong enough to make the electron Larmor radius much smaller than the discharge chamber length but not so strong as to affect ion trajectories. Ions are not influenced by the magnetic field because the ion mass is many orders of magnitude larger than the electron mass [11].

The third major component, the discharge chamber, electrically isolates the plasma from the metallic parts of the thruster and is composed of an insulating ceramic such as BN. The discharge chamber is where the propellant is ionized. The electrons that collide with the propellant in the discharge chamber originate from the cathode. The electric potential gradient is largest in the final section of the chamber owing to the low electron axial mobility in this restricted area. This potential gradient accelerates the ions to very high speeds which generates the plasma plume and subsequently thrust [6].

Ions exiting the thruster encounter additional electrons from the fourth major component, the cathode. The cathode supplies electrons to the exhaust plume for neutralization of the space charge downstream of the thruster as well as to the discharge chamber for propellant ionization [9]. A typical cathode is constructed from a hollow tube with a propellant gas inlet and a small orifice at the outlet. The inside wall of the cathode is lined with a low work function material that produces electrons by thermionic emission when heated. Materials such as porous tungsten impregnated with barium or lanthanum hexaboride are typically used [6]. Inside the cathode, thermionic electrons collide with propellant from a dedicated gas source and create plasma. The thermionic and secondary electrons are then extracted through the exit orifice using a positively biased electrode called a keeper [11].

Most flight qualified Hall thrusters are designed with two cathodes in order to provide redundancy should one cathode fail on orbit [12]. Figure 1.2 contains a photograph of a Snecma

PPS-1350 flight qualified Hall thruster, with redundant cathodes, capable of producing 90 mN of thrust [13]. Of note in the figure are the position of the cathodes and the smooth channel walls near the exit plane of the thruster. Cathode positioning and wall material sputtering will be discussed in subsequent sections.



Figure 1.2. Snecma PPS-1350 Hall thruster used on commercial satellites [13].

Xe is the propellant gas typically used in Hall thrusters because of its high molecular weight, non-toxic and non-corrosive properties and relatively low (first) ionization level of 12.23 eV [14], [15]. While Xe is the propellant gas of choice, Hall thrusters can also be operated on other noble gases such as Krypton (Kr) and Argon (Ar) [6].

1.2. Governing Equations

The electromagnetic phenomenon that causes electrons to orbit the magnetic core, and thus create the Hall effect that the thruster is named for, is called the Lorentz Force Law. The Lorentz Force Law describes the force on a charged particle due to the presence of electric and magnetic fields. The Lorentz force, \vec{F} , is defined as:

$$\vec{F} = q[\vec{E} + \vec{v} \times \vec{B}] \quad (1.1)$$

where q is the charge on the particle, \vec{E} and \vec{B} are the electric and magnetic field vectors, respectively, and \vec{v} is the particle's velocity vector. The Hall effect is due to electrons moving perpendicular to the electric field and around the magnetic core under the influence of the magnetic field. A component of the overall force on the charged particle comes from the resultant of the cross product between the particle's velocity and the magnetic field. The magnetic field always acts perpendicular to an electron's velocity and therefore cannot change the energy of the particle, i.e. accelerate/decelerate the particle. However, the magnetic field can affect the direction of the particle's motion. Electrons on their circular path collide with neutral propellant atoms and create ions. Because of the electric potential applied between the anode and the exit plane, an electric field is created that accelerates the ions.

When the ions exit the thruster, they create a thrust force in the opposite direction [15]:

$$Thrust = \dot{m}_{propellant} \cdot v_{exit} \quad (1.2)$$

where $\dot{m}_{propellant}$ is the propellant mass flow rate and v_{exit} is the average ion exit velocity defined as:

$$v_{exit} = \sqrt{\frac{2 \cdot q \cdot V_b}{M}} \quad (1.3)$$

where q is the ion's charge, V_b is the effective voltage the ion was accelerated through and M is the ion mass. Typical ion exit velocities are between 10 - 30 km/s depending on the thruster size, power input, applied voltage and mass flow rate. Hall thrusters produce between 30 mN to 3 N of thrust depending upon power input level and ion exhaust velocity [6], [9].

The kinetic energy of the ion exhaust is called the jet power (P_{jet}) [6]:

$$P_{jet} = \frac{1}{2} \dot{m}_{propellant} \cdot v_{exit}^2 \quad (1.4)$$

Using Equation 1.2, the jet power becomes

$$P_{jet} = \frac{Thrust^2}{2 \cdot \dot{m}_{propellant}} \quad (1.5)$$

Ideally, every propellant atom that enters the discharge chamber would be ionized by an electron collision and exit the thruster to produce thrust. However, in an actual thruster not all input power is converted to thrust and all propellant atoms are not ionized and accelerated. The thruster efficiency ($\eta_{thruster}$) is defined as the power out (jet power) divided by the total electrical power input (P_{input}) [15].

$$\eta_{thruster} = \frac{P_{jet}}{P_{input}} \quad (1.6)$$

Substituting 1.5 into 1.6 yields

$$\eta_{thruster} = \frac{Thrust^2}{2 \cdot \dot{m}_{propellant} \cdot P_{input}} \quad (1.7)$$

This is the preferred equation for calculating the thruster efficiency as the thrust, propellant mass flow rate and input power can all be measured and monitored during thruster operation. Typical thruster efficiencies are between 45% and 65%. Several mechanisms cause the thruster to operate at less than ideal conditions. First, part of the input power is transferred to the propellant as heat or excites the propellant without ionizing it. Additionally, part of the input power is lost when ions strike and recombine on the chamber walls. These collisions neutralize the ions thus causing the need for another neutral-electron collision to recreate the ion while also causing an increase in wall temperature and wall material sputtering [10].

1.3. Propulsion Characteristics

Hall thrusters produce low thrust over prolonged periods to execute orbital maneuvers for satellite station keeping or space exploration. Hall thrusters are gaining popularity over chemical thrusters due to their high specific impulse and owing to their significant advantage of using less propellant than conventional chemical thrusters. Specific impulse (I_{sp}) is defined as [16]:

$$I_{sp} = \frac{Thrust}{\dot{m}_{propellant} \cdot g_{eo}} \quad (1.8)$$

where g_{eo} is the acceleration due to gravity measured at the surface of the Earth. Specific impulse, expressed in units of seconds, can be loosely described as the fuel economy rating of a thruster. Instead of using a ratio of distance and fuel consumption, specific impulse uses a ratio of thrust and fuel consumption. For example, for a given thrust, a high specific impulse thruster will use less propellant than a low specific impulse thruster. Or conversely, for a given amount of propellant, a high specific impulse thruster will have more thrust over a low specific impulse thruster. Specific impulse values for chemical rockets are around 300 – 450 s while values for Hall thrusters are around 1300 – 1600 s and can be as high as 3000 s [9]. However, most Hall thruster sizes are referenced by their input power requirement expressed in either Watts or Kilowatts. An example of this is the BHT-200 which (nominally) requires 200 W of input power and produces 12.8 mN of thrust at an I_{sp} of 1390 s [15].

1.4. History and Development

Hall thrusters were first used in December 1971 when the Soviet Union launched the satellite “METEOR” with two SPT-50 Hall thrusters as the primary station keeping propulsion system. The Soviet Union and Russia have since flown over 140 Hall thrusters in their satellite programs [17]. The prefix “SPT”, meaning Stationary Plasma Thruster, is translated from Soviet literature, but refers to the continuous operation (“stationary”) of Hall thrusters in comparison to Pulsed-Plasma Thrusters (PPT) that they had previously tested and flown in the 1960s. Since the beginning of the Space Race, the Soviet Union has had a keen interest in Hall thrusters while the US focused mostly on chemical thrusters with smaller research efforts on gridded ion thrusters [6].

Hall thrusters did not start gaining popularity in the US until after the breakup of the Soviet Union in 1991. Organizations such as NASA's Jet Propulsion Lab, the Air Force Research Lab (AFRL) and Space Systems/Loral became interested in the reliability, performance and flight records of Russian designed Hall thrusters. Scientists and engineers obtained Russian Hall thrusters to verify performance claims and gain a better understanding of their technology. In October 1998, the Naval Research Lab's experimental "STEX" spacecraft was launched with a Russian built D-55 Hall thruster. This marked the first western use of Hall thrusters and started significant efforts towards developing domestically designed and built Hall thrusters [18]. In December 2006, the US launched its first satellite with domestically designed and built Hall thrusters. Specifically, the AFRL test bed satellite "TacSat-2" had BHT-200 Hall thrusters on board for demonstration and testing purposes [19].

Today, Hall thrusters are found on many commercial geosynchronous satellites for orbit insertion and station keeping and are also gaining popularity with the US military. In August 2010, the Air Force launched the first in a series of satellites for its Advanced Extremely High Frequency (AEHF) satellite program. These AEHF satellites were the first US military satellites to utilize Hall thrusters for station keeping. The four geosynchronous satellites in the AEHF constellation each have four Aerojet BPT-4000, 4.5 kW Hall thrusters [20], [21]. Figure 1.3 illustrates an AEHF satellite being prepared for nose cone integration and launch. A BPT-4000 Hall thruster can be seen on the corner, mid-way up the satellite. Using Hall thrusters over chemical thrusters resulted in each satellite having over 2000 lbs of weight savings because of the decreased propellant mass requirements. These weight savings allowed the satellite designer to increase the payload size allowing a larger communications suite [21].



Figure 1.3. BPT-4000 mounted on an AEHF satellite during launch preparation [22].

1.5. Thruster Channel Material Properties

The Boron Nitride (BN) material used to construct the walls of Hall thrusters is a ceramic created by hot pressing high purity BN powder at temperatures around 2000°C and pressures around 2000 psi. The grade of BN typically used is known as HBC, standing for Hot-pressed Boron Nitride, Chemically purified. During hot pressing, the BN molecules are diffusion bonded without using a binder resulting in a material with minimal moisture absorption characteristics. Although BN is machinable, it's often pressed into the desired final shape and unlike metal materials, requires no additional heat treatment to obtain its final characteristics. HBC BN has a hexagonal crystal structure and is often referred to as hexagonal BN or h-BN. This crystal structure results in HBC BN having high thermal conductivity and low thermal expansion properties and can be used in applications up to 3000°C. HBC BN is an excellent electrical insulator, it's non-toxic, has high oxidation and chemical resistance and has a low density [23].

1.6. Sputter Erosion in Hall Thrusters

Reliable knowledge of thruster lifetimes and variations of performances during thruster lifetimes are crucial for planning of flight missions and optimization of the propulsion systems [18]. Long duration testing is an important method for validating thruster lifetime and performance. However, long duration testing of Hall thrusters to the point of material failure, known as full life testing, is extremely time consuming, resource intensive and very expensive. The erosion of the Hall thruster channel walls from ion impingement and subsequent sputtering is the most important life-limiting factor for Hall thrusters [24]. An objective of this research is to demonstrate the use of CRDS to measure the amount of sputtering of thruster wall material.

Sputtering is the term used to describe the molecular level interaction occurring when a molecule or charged particle collides with a solid surface and liberates particles from that surface. This collision can take on many forms from an almost elastic collision to particle implantation into the solid. The collision type of most interest to this research is when a particle, in this case a Xe ion, collides with the solid thruster wall and ejects atoms or molecules. This phenomenon is described in the following section. After many collisions occurring over repeated thruster firings, the wall material eventually thins to the point of complete erosion leading to thruster failure.

1.6.1. Mechanisms of Physical Sputtering

When the Hall thruster wall material is bombarded with ions possessing kinetic energies exceeding the material's lattice displacement energy, molecules in the wall may be pushed into new positions. This internal rearrangement results in a cascade of internal collisions in all directions within the wall material. When the cascade of collisions reaches the surface with

energy greater than the surface binding energy, a surface atom or molecule will be ejected from the material. This process is known as physical sputtering or more simply, sputtering [25].

The cascade effect in the wall material from an incident ion is a complicated event and here we summarize a few fundamental concepts. If an incident ion possesses less energy than the wall material's lattice displacement energy and does not impart sufficient energy to a surface atom or molecule to overcome its surface binding energy, no sputtering of molecules within the bulk of the material or the surface will occur. Conversely, when an incident ion possesses energy above 10 keV, the ion tends to implant itself into the wall material and causes a cascade of collisions away from the surface of the material. In both cases, the sputter yield of the wall material is very low. Energies between these two extremes are of greater interest. In fact, incident ions with energies between 60 – 500 eV are found in the plasma contained in the discharge chamber of Hall thrusters. They produce measureable sputtering of the walls and are therefore the ion energies of interest to this research [26].

As the ion incidence angle changes, so does the cascade of collisions and subsequent sputtering behavior of the wall material. The ion incidence angle is the relative angle measured from the surface normal to the path the ion travels prior its collision with the wall. Inside Hall thrusters, ions impact the walls from glancing angles to normal incidence. Khartov et al. found that for BN, incidence angles that produces the maximum sputtering are typically around 50° [27].

Total sputter yields are often expressed in units of cubic millimeters per Coulomb (mm^3/C). These units represent a volume of sputtered material per Coulomb of charge of the incident ions. These units are preferred over units of sputtered atoms per incident ion (atoms/ion) because determining whether the sputtered materials are atoms, molecules or a

combination of both is avoided [28]. Additionally, when the sputter yields of multi-component materials such as BN are compared to single component materials such as Molybdenum, units of mm^3/C make for a cleaner comparison.

Rubin et al. have published measurement of HBC BN sputter yields at incident ion energies between 60 – 500 eV and incidence angles between 0° and 45° . Their sputter yield measurements were found as low as $0.0145 \text{ mm}^3/\text{C}$ at an incident ion energy and angle of 60 eV and 0° , respectively to as high as $0.125 \text{ mm}^3/\text{C}$ at 500 eV and 45° [29]. The latter measurement is a significant amount of sputtering. Should plasma in a discharge chamber possess those characteristics, it would cause noticeable damage to the thruster wall material.

The last fundamental concept of concern is the region within the thruster that experiences the most sputtering. The walls of Hall thrusters tend to preferentially sputter and subsequently erode in a region around the exit plane known as the acceleration zone. A Hall thruster with severe wall erosion in its acceleration zone is illustrated in Figure 1.4.

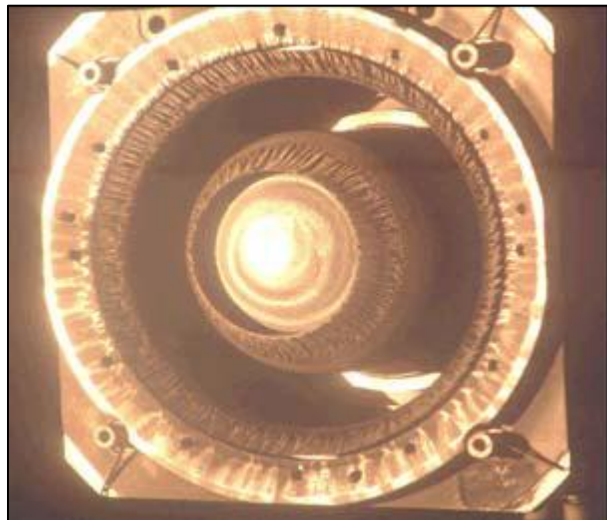


Figure 1.4. Hall thruster with severe wall erosion in its acceleration zone [15].

The acceleration zone corresponds to the region along the thruster axis with the greatest electric field gradient. This large gradient occurs because the electrons orbiting in this region have low

axial mobility due to the large magnetic field near the thruster exit. In this zone, ions reach extremely high velocities and exit the thruster [10]. However, during acceleration, some ions get divergent trajectories relative to the thruster axis and collide with the thruster walls resulting in wall material sputtering [15].

Abgaryan et al. performed lifetime tests on a SPT-100 Hall thruster and found that after 4,000 hours of operation, approximately 30 cm^3 of wall material had been sputtered. This material removal caused the channel width to change by 10%. Sputtered material exiting spacecraft thrusters can potentially erode or deposit on various spacecraft components such as antennas, solar panels and optics. Over time, the deposited material could cause spacecraft component functions to degrade or fail [30]. Additionally, the increase in discharge chamber volume as well as the evolving wall shapes due to sputtering increases the probabilities that neutral atoms exit the thruster without becoming ionized, causing declines in thruster efficiency [31].

1.7. Problem Statement

In electric propulsion testing and research, vacuum facilities simulate space conditions that Hall thrusters on spacecraft experience on orbit. These facilities provide a means to operate Hall thrusters for purposes of testing thruster performance and characterizing their plasma. The Colorado State University (CSU) Laser and Plasma Diagnostics Lab (LPDL) needs a vacuum facility capable of testing and characterizing low power ($\lesssim 600 \text{ W}$) Hall thrusters. The LPDL's need for such a facility is the problem that this research effort solves. During this research effort, a small vacuum chamber capable of maintaining pressures of 5×10^{-5} Torr or lower while operating a SPT-70 Hall thruster on Xe gas is assembled. Additionally, a portion of this research

effort focuses on proof-of-principle sputter erosion measurements using the laser-based Cavity Ring-Down Spectroscopy (CRDS) technique.

Pressures in low to geosynchronous earth orbit range from 5×10^{-6} to 5×10^{-10} Torr [5]. However, it is generally accepted that pressures around 5×10^{-5} Torr are acceptable for thruster experimentation excluding full lifetime testing [32]. Chamber pressure of 5×10^{-5} Torr or lower are desired so that the thruster's discharge current is not influenced by the ingestion of the background chamber gases entering from the plume side of the thruster. An ingestion rate of 3% or less of the thruster flow rate is acceptable. However, if the chamber background pressure rises much above 5×10^{-5} Torr, the ingestion rate of the thruster will rise above 3% and may cause questionable performance of the thruster [32]. At pressures above 5×10^{-5} Torr, the propellant mass flow rate is artificially elevated due to this ingestion. The additional ions created are from an artificial source and subsequently give false gains in performance, operation and plume characteristics [5]. Therefore, a vacuum chamber with sufficient pumping speed and operating pressure is needed to appropriately test Hall thrusters.

There are several objectives of this research effort that will result in meeting the LPDL's need for a vacuum facility to test Hall thrusters. The objectives are as follows:

- Assemble a small vacuum chamber from donated materials specifically to operate a SPT-70 Hall thruster at high vacuum with Xe flow rates up 30 sccm.
- Provide the chamber with more than the minimum required pumping speed of 8,000 L/s to operate the SPT-70 at a pressure no higher than 5×10^{-5} Torr.
- Configure the chamber and thruster mounting scheme such that there is optical access to the thruster's exit channel in order to allow CRDS of the exhaust plume.
- Install supporting equipment and demonstrate initial thruster operation.

- Measure ion current density of the plume to understand thruster operation.
- Conduct initial CRDS measurements of sputtered Boron from the channel walls.

1.8. Thesis Layout

The remainder of this thesis is organized as follows. Chapter 2 details the development of the HTECh to include description of the chamber cryogenic pumps, operating principles and estimated and measured pumping speeds. Chapter 3 outlines SPT-70 operation, tests and results and includes specific information on procedures used to operate the thruster (included also as Appendices A & B). Chapter 4 describes the laser-based diagnostics used to examine the thruster's exhaust and includes preliminary results. Chapter 5 presents concluding thoughts on the research accomplished and is followed by the list of references used throughout the thesis in Chapter 6.

2.0 DEVELOPMENT OF THE HTECh

The HTECh was assembled from vacuum facility equipment donated to the university by the AFRL on Wright-Patterson Air Force Base. Modifications to include welding and machining were needed to reconfigure the chamber to install three cryogenic pumps and incorporate CRDS optical components. Lab renovations and upgrades were needed to provide the necessary access, power and water needed for chamber operation. The chamber was thoroughly cleaned prior to assembly and wiring of its control panels. The three cryogenic pumps were cleaned and refurbished prior to being installed on the chamber. A system to mount, fuel and power the thruster was also built and incorporated into the chamber. All chamber components were tested to ensure the appropriate high vacuum condition for a thruster operating with up to 30 sccm of Xe was achieved. Finally, the SPT-70 was operated and tested in the chamber.

2.1. Components and Design

The chamber donated to the university was previously used by the AFRL as a Large Area Deposition System (LADS) chamber for ion-beam deposition studies. Figure 2.1 illustrates the LADS chamber with the main components labeled at the AFRL prior to disassembly and transport to CSU. The main three foot diameter, four foot long chamber was connected to a one and a half foot diameter, two foot long load lock chamber with a sample transfer mechanism that was used to insert and position substrate materials. The load lock provided the ability to access and set-up the substrates and then transfer them while keeping the main chamber under continuous vacuum. Vacuum conditions were created using two Cryo-Torr® (CT) 10 cryogenic pumps as well as one Varian TV 1001 Navigator turbo pump resulting in a total pumping speed of approximately 3,500 L/s of Xe. The chamber was supported by various equipment such as ion

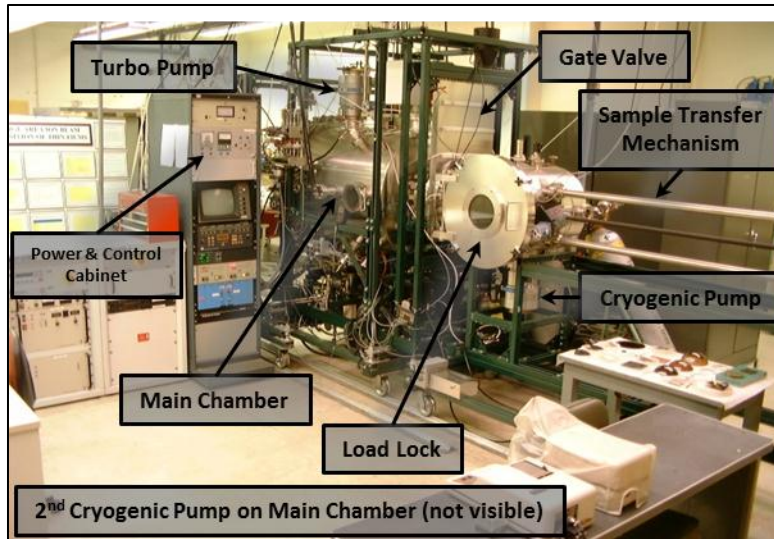


Figure 2.1. The LADS chamber at the AFRL prior to disassembly.

source power supplies, pneumatic control valves, a quadrupole gas analyzer, vacuum and temperature gauges, gas flow controllers and a cooling water system.

An ion source was located at one end of the chamber and a multi-degree of freedom target positioning mechanism was installed in the center of the main chamber. The load lock was separated from the main chamber by a 20 inch pneumatically controlled gate valve used for isolation when needed. The chamber also had a 10 inch pneumatic gate valve used to isolate one of its cryogenic pumps when needed.

The donated chamber and equipment was very robust and mostly a complete system, however, it was in desperate need of a thorough decontamination and cleaning. Figure 2.2 illustrates the main section of the LADS chamber upon arrival to CSU.

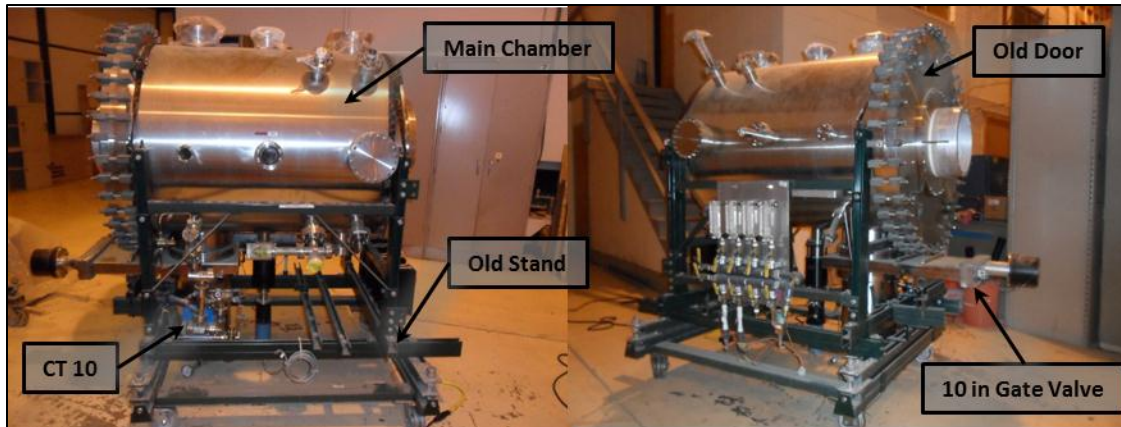


Figure 2.2. LADS main chamber after disassembly and transport to CSU.

The inside of the chamber was coated with creosote like deposited material that required removal by manual means. The entire attached vacuum plumbing system to include the cryogenic pump, required complete disassembly and cleaning. It was additionally determined that any chamber modifications would have to include a stronger and more rigid supporting frame as well as changing the large bolted-door flange into a hinged door.

After inventorying and reviewing all the donated equipment, a plan to reconfigure the chamber was established. Due to space restrictions in the lab, the load lock and sample transfer mechanism were eliminated from the design. However, the gate valve that was used to isolate the chamber from the load lock was repurposed to go between the chamber and a large cryogenic pump. The 10 inch cryogenic pump and its gate valve would remain in their original location and an additional cryogenic pump would be added to the door side of the chamber.

To accommodate the large cryogenic pumps at each end of the chamber, welding and machining was necessary. To accomplish this, a local machine shop, Precision Machined Products, was contracted to make several significant modifications to the chamber. These modifications included changing the bolted door to a hinged door capable of mounting a cryogenic pump, welding adapter flanges to the 20 inch gate valve, facing all large flanges,

machining grooves for O-ring seals between all mounting surfaces and building a new support frame. Figure 2.3 illustrates the chamber on a large horizontal mill while a groove for an O-ring on the door flange is machined.

These modifications allowed the chamber to be fitted with three cryogenic pumps that will be described in a subsequent section. The door reconfiguration allowed easy chamber access because the entire end of the chamber could now be opened. The adapter flanges allowed a seamless integration from a cryogenic pump thru the 20 inch gate valve to the chamber. Lastly, the new support frame integrated caster wheels used during delivery and positioning as well as adjustable feet and outriggers for floor installation.



Figure 2.3. Groove for O-ring being machined into the door flange.

Figure 2.4 illustrates the chamber after the 20 inch gate valve was installed and while still on its caster wheels used during chamber delivery.



Figure 2.4. HTECh after gate valve installation and positioning.

Concurrent to the machining process, all three cryogenic pumps (CT 10 and two CT 500s) received much needed refurbishment. The internal components of these donated cryogenic pumps were in complete disrepair and one pump was missing all of its internal components. It was decided to completely rebuild two of the three pumps and modify the third pump with custom internal components. All three cold heads were completely disassembled, cleaned and rebuilt with new seals and bearings and all compressor adsorbers were replaced.

In addition to the chamber upgrade and reconfiguration, facility upgrades were needed to accommodate the chamber and its supporting equipment. Several single and three phase, 120 V and 220 V circuits were installed for the three cryogenic pump compressors, power supplies and controllers necessary to operate the chamber. Cooling water supply and return lines were installed to cool the three cryogenic pump compressors. An air compressor and associated pneumatic lines were installed to operate the gate valves. Laboratory rearrangement was necessary to make room for the new chamber, associated equipment and an optical table for laser

measuring equipment. Additionally, a new lab access door was installed in order to allow movement of the chamber into the room. Lastly, once the chamber was positioned, it required bolting to the floor so that the weight of the door would not cause the chamber to tip over when it was opened. Figure 2.5 illustrates the chamber, with the main components labeled, in its permanent location in the lab.

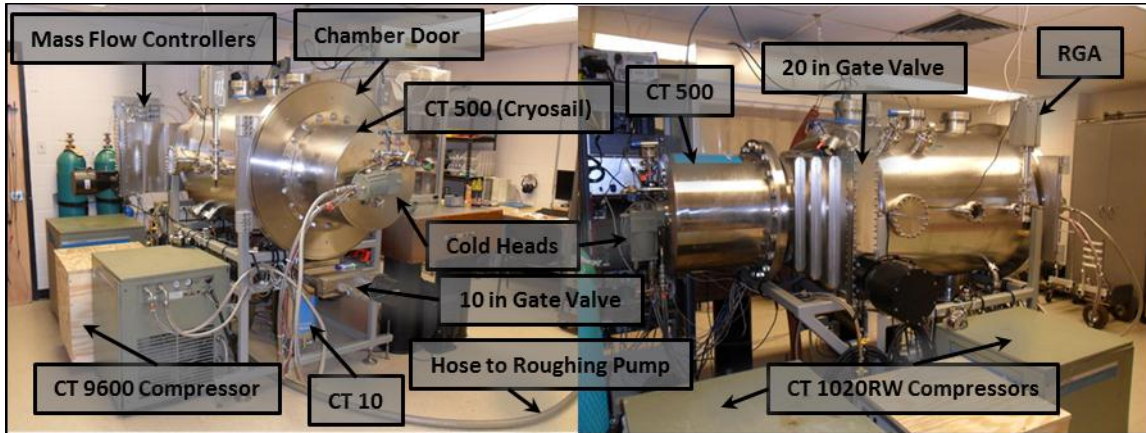


Figure 2.5. HTECh after assembly and installation.

After all modifications, reconfiguration, installation and operational tests were complete and ultimate base pressure of 4×10^{-8} Torr was achieved. Component specifications of the HTECh (labeled in Figure 2.5) are outlined in Table 2.1. Cryogenic pump descriptions and pumping speed calculations are included in the next section.

Table 2.1. Summary of HTECh feature.

Chamber Dimensions (main chamber)	3 ft diameter by 4 ft long (0.914 m diameter by 1.22 m long)
Chamber Volume	880 Liters (31.1ft ³)
Cryogenic Pumps	CT 500, CT 10, Cryosail (modified CT 500)
Total Pumping Speed	15,620 L/s (Ar) 10,500 L/s (Xe)
Ultimate Base Pressure	4x10 ⁻⁸ Torr (calibrated for N ₂)
Roughing Pump	Trivac Duel Stage Rotary Vane Pump
Gate Valves	20 in NorCal Products gate valve between CT 500 and chamber 10 in MDC Vacuum Products gate valve between CT 10 and chamber
Pressure Gauges	2x Granville Phillips Convection Gauges 1x Granville Phillips Ion Gauge
Cryogenic Pump Temperature Sensors	1x on second stages of CT 500 & CT 10, 1x on second stage and 1x on finger of Cryosail
Mass Flow Controllers (w/bypass valve installed for pump down)	3x Unit Instruments 7360
Residual Gas Analyzer	1x SRS RGA 100
Cross Over Pressure (pressure at which gate valves are opened during pump down)	P _{cross} = 0.57 Torr (CT 500) P _{cross} = 0.34 Torr (CT 10)

2.2. Cryogenic Pumps

The HTECh was outfitted with three cryogenic pumps each with their own He compressor. Three cryogenic pumps are used to create high vacuum in the chamber as well as provide sufficient pumping speed to capture the expended Xe used to operate the Hall thruster. A CT 500 was mounted to the backside of the 20 inch gate valve and is fed by a water cooled CT 1020RW compressor that supplies He to its cold head at 270 psi. A CT 10 was mounted to the bottom of the 10 inch gate valve and is fed by a water cooled CT 9600 compressor supplying He to its cold head at 150 psi. Both of these cryogenic pumps are mounted behind gate valves such that their vacuum vessels can be isolated and remain at vacuum during times when the rest of the chamber is exposed to the atmosphere for material and experiment set-up.

An additional cryogenic pump was mounted on the door and protrudes into the chamber. This pump is a CT 500 cryogenic pump modified with custom internal components and is referred to as the cryosail. The cryosail is fed by the same type of He compressor as the CT 500, however it is not behind a gate valve. Due to its configuration, the cryosail must be warmed to room temperature prior to each time the chamber is exposed to atmospheric conditions. Warming the cryosail to room temperature prior to chamber venting prevents the water in the room air from condensing and later thawing and contaminating the chamber. The cryosail is discussed in detail in the next section.

Cryogenic pumps operate on the principle that gases can be condensed on a surface or trapped in a carbon matrix at extremely low temperatures [33]. The cold head maintains these collecting surfaces, called arrays, at cryogenic temperatures by a two stage, controlled expansion of pressurized He in cycle called the Gifford-McMahon refrigeration cycle [34]. Traditional cryogenic pumps are designed to remove a variety of gases by maintaining their two stages and associated arrays at two distinct temperatures.

The first stage temperature is approximately 80 K (-316 °F), and the second stage temperature is approximately 15 K, (-433 °F). These extremely low temperatures are achieved by the rapid expansion of pressurized He in the cold head cylinder at the core of the pump's vacuum vessel. There is a set of arrays attached to the first stage and several other sets of arrays attached to the second stage. By way of conduction heat transfer, the arrays are cooled to extremely low temperatures. These arrays either freeze or trap gases and therefore remove them from the chamber. The bottom sides of the second stage arrays are covered in charcoal for purposes of trapping gases that will not freeze. This method of trapping is known as adsorption [35].

Adsorption, not to be confused with absorption, is the adhesion of atoms or molecules of gas to the surface of a material. Adsorbent materials, such as activated charcoal, are porous and provide large surface areas for gases to adhere. This differs from absorption, in which the gas permeates or is dissolved into the material and makes a solution. The adhesion between the adsorbent material and the gas (adsorbate) is weak. This adhesion is easily reversible by heating the adsorbent material to release the adsorbate [36].

The two sets of arrays are held at different temperatures so that water vapor and hydrocarbons freeze to the first stage arrays and Oxygen (O / O_2), Nitrogen (N / N_2), Argon (Ar), Helium (He), Hydrogen (H) and Neon (Ne) either freeze or adsorb to the second stage arrays. Arrays and other internal components of a typical cryogenic pump vacuum vessel are illustrated in Figure 2.6.

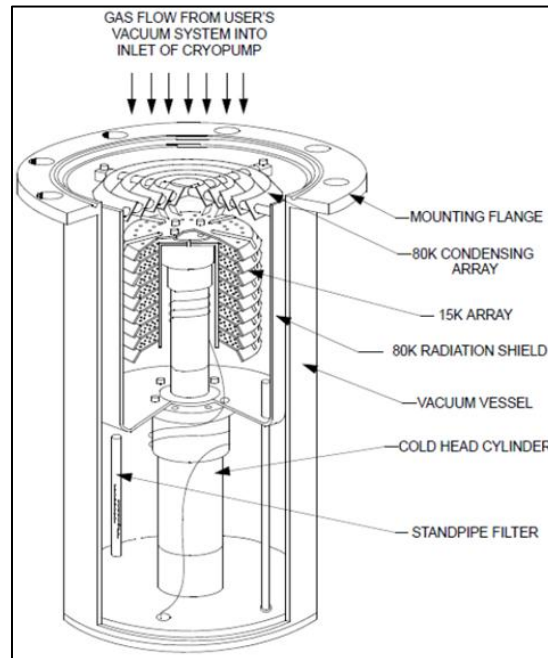


Figure 2.6. Typical cryogenic pump vacuum vessel internal components [33].

In the case of the second stage arrays in the vacuum vessel, H, He and Ne contact the arrays and are cooled to temperatures of around 15 K. Upon contact, the gases lose most of their

incident kinetic energy and are trapped by adherence to the adsorbent material. This trapping technique is used over attempting to condense these three gases as that requires much more sophisticated equipment to reach even lower temperatures [34].

2.3. Cryosail Construction

As stated, custom internal components were built for one of the CT 500 cryogenic pumps. Since there are two other cryogenic pumps attached to the chamber plenty capable of removing a variety of gases, it was decided that it would be advantageous to have a pump specifically designed to remove the heavier gases commonly used with Hall thrusters. Specifically, it was anticipated that the Hall thruster would operate primarily on Xe, Ar or Kr. The principle of the cryosail is to use a large surface area maintained at cryogenic temperatures to collect these three noble gases and maintain the chamber at high vacuum. These large surface areas are referred to in the “sail” portion of the cryosail name.

Since the broader objective of this research effort was to commission a vacuum chamber in a timely manner, it was decided to approach the cryosail design and construction with criteria of simplicity, availability of materials and ease of construction. The dimensions of the CT 500 housing and the availability of stock sized material drove the design of the internal components. Figure 2.7 illustrates renderings of the cryosail with its main components labeled. The final design met the above design and construction criteria.

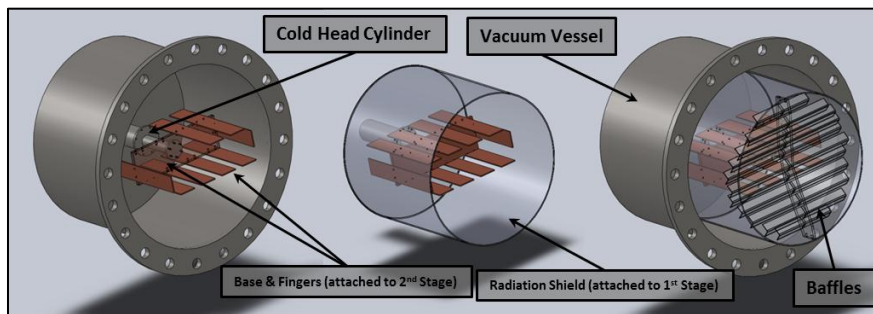


Figure 2.7. Renderings of the cryosail highlighting various components.

The cryosail base and fingers are made out of copper and are attached directly to the second stage of the cold head cylinder such that, by conduction heat transfer, these pieces reach 15 K. The cryosail base and fingers attached to the cold head cylinder inside the CT 500 vacuum vessel can be seen in the left picture of Figure 2.7. A radiation shield made from aluminum was added around the cryosail base and fingers and attached to the first stage of the cold head cylinder such that, by conduction heat transfer, it reaches 80 K. The radiation shield attached to the first stage of the cold head cylinder can be seen in the middle picture of Figure 2.7. Aluminum baffles were added to the entrance of the cryosail and attached to the radiation shield as seen in the right picture of Figure 2.7. These baffles serve to limit the radiation heat transfer from the chamber to the copper surfaces maintained at 15 K while only slightly restricting the molecular flow entering the cryosail.

All the materials used to construct the cryosail were from stock sized material procured through common material vendors. The radiation shield was made from a modified aluminum food-grade batch can and the copper and aluminum were purchased in standard lengths. All parts were machined at the university including the baffle center bracket that was made using a water jet. Since the pumping speed of the cryosail could only be estimated during design, the baffles and fingers were designed to be removable to make configuration adjustments easy. The cryosail was assembled in the chamber with indium foil between all mating surfaces. The cryosail base and fingers maintained surface temperatures of 15 K to 20 K with area of 0.38 m^2 , while the radiation shield is maintained at temperature 80 K with area of 1.46 m^2 .

Two silicon diode temperature sensors (CT P/N 8080250K012) were installed on the cryosail to monitor the temperature at the cryosail base and the tip of one of the fingers farthest from the second stage of the cold head cylinder. The cryosail performed very well after a three

hour cool down period. The cryosail base and finger reached and maintained a temperature of 16 K and 20 K respectively. However, after several pumping speed tests, outlined in the following section, it was determined that removing the baffles was necessary to get a higher pumping speed. The final cryosail configuration used in the HTECh is shown in Figure 2.8.

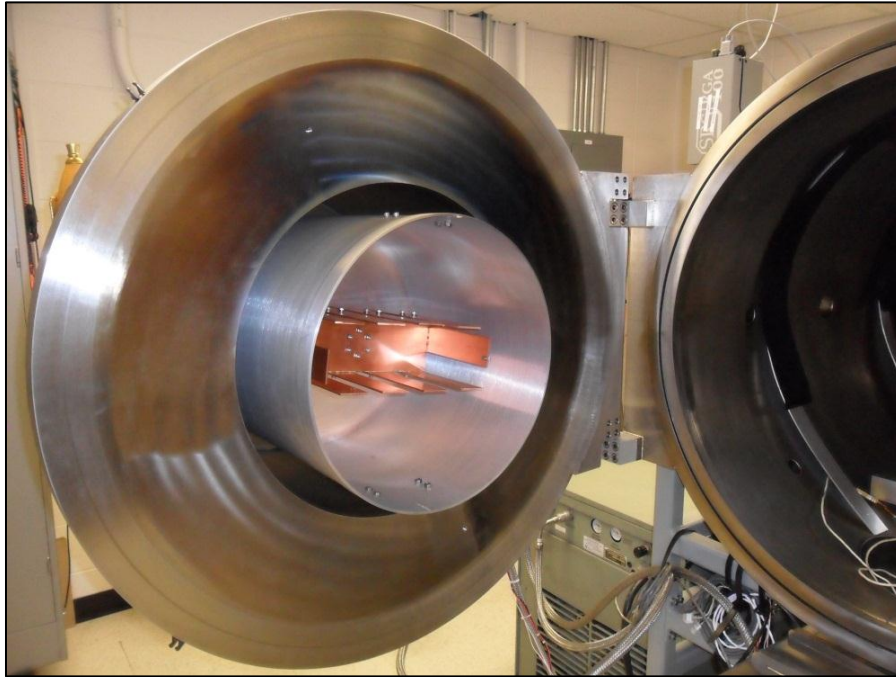


Figure 2.8. Final cryosail configuration used in the HTECh.

2.4. Estimated Pumping Speeds

Here we present preliminary estimates of the anticipated HTECh pumping speeds and resulting chamber pressure during thruster operation. These preliminary estimates were done to ensure the final cryogenic pump and chamber configuration would provide sufficient vacuum capabilities to operate a SPT-70 Hall thruster as discussed in section 1.7. The pump speed estimates were based on published pump speed data and accounting for the conductance losses owing to the reduction in area of the pumps' flanges. A similar estimation was done for the cryosail and then all three effective pumping speeds were summed to get the total pumping speed

of the chamber. The procedure and associated equations are in the following section. A summary of the estimated pumping speed calculations are in Table 2.2 in section 2.4.3.

2.4.1. CT 10 and CT 500 Pumping Speed Calculations

When operating with different gases, cryogenic pump speeds are scaled using molecular weights [37]:

$$S_{Xe} = S_{Air} \sqrt{\frac{MW_{Air}}{MW_{Xe}}} \quad (2.1)$$

where S_{Xe} is the pumping speed on Xe, S_{Air} is the pumping speed for air (found from published data) and MW_x are the corresponding molecular weights. Published pumping speed data for the CT 10 and CT 500 for air is converted to Xe pumping speed using Equation 2.1. The conductance loss from the flanges (apertures) connecting the pumps to the chamber is found as [38]:

$$C_{aperture} = \left(\frac{A}{4}\right) \sqrt{\frac{8 \cdot R \cdot T_i}{\pi \cdot MW_{Xe}}} \quad (2.2)$$

where A is the cross sectional area of the inside flange diameter, R is the ideal gas constant and T_i is gas temperature. Conductance losses are used in conjunction with the pumping speeds found for Xe to find the effective pumping speed for each pump/flange combination. Equation 2.3 is used to find the effective pumping speed for each cryogenic pump [38]:

$$S_{eff} = \left(\frac{1}{S_{Xe}} + \frac{1}{C_{aperture}}\right)^{-1} \quad (2.3)$$

2.4.2. Cryosail Pumping Speed Calculation

The theoretical pumping speed, S_{th} , of the cryosail is estimated using a technique published by Rutledge et al. [39]:

$$S_{th} = \left(\frac{T_i R}{2 \cdot MW_{Xe}} \right)^5 \left[1 - \frac{P_c}{P_i} \left(\frac{T_i}{T_c} \right)^5 \right] A_c \quad (2.4)$$

where T_i is the temperature of the pumped gas, T_c is the cryosail temperature, P_c is the vapor pressure of the pumped gas at T_c , P_i is the vacuum chamber pressure and A_c is the surface area of the cryosail. This estimation results in a (high) theoretical pumping speed of 36,570 L/s. However, the conductance of the aperture leading to the cryosail must also be taken into account to determine the effective pumping speed (Equations 2.2 and 2.3). The results of these calculations are summarized in Table 2.2.

2.4.3. Summary of Estimated Pumping Speed Calculations

Table 2.2 summarizes the results of estimating the pumping speeds for each of the cryogenic pumps used in the HTECh. The total effective pumping speed of the HTECh is estimated to be 10,860 L/s.

Table 2.2. Summary of Estimated Pumping Speed Calculations.

Cryogenic Pump	S_{Air} [33]	S_{Xe}	$C_{aperture}$	S_{eff}
CT 10	3,000 L/s	1,410 L/s	3,700 L/s	1,020 L/s
CT 500	10,000 L/s	4,700 L/s	8,260 L/s	3,000 L/s
Cryosail	n/a	36,570 L/s	8,420 L/s	6,840 L/s
			Total S_{eff}	10,860 L/s

The anticipated theoretical pressure of the HTECh during operation of the SPT-70 is found as [40]:

$$P_{HTECh} = \frac{Q}{S_{eff}} \quad (2.5)$$

where Q is the throughput of the system found (i.e. mass flow rate of the SPT-70) and S_{eff} is the total effective pumping speed. The maximum flow rate of the SPT-70 and its cathode is anticipated at 30 sccm. The anticipated theoretical pressure of the HTECh during operation of the SPT-70 and its cathode is therefore estimated as 3.5×10^{-5} Torr on Xe. This is an acceptable

chamber pressure to conduct testing on Hall thrusters and is similar to pressures found in published data for past Hall thruster performance measurements (see section 1.8).

2.5. Pumping Speed Test Results

To confirm the chamber pressure during Hall thruster operation as well as validate the estimates, the pumping speeds of the three cryogenic pumps were measured. The pumping speeds were found from experiments in which Xe was introduced into the chamber at increasing flow rates while the pressure was recorded for different flow rates.

During the experiments, the pressure data was recorded using a pressure sensor calibrated for nitrogen. Therefore, it was necessary to correct the data to pressure measurements of Xe. The pressure correction (in units of Torr) is found as [5]:

$$P_{Xe} = \frac{P_{N_2} - P_b}{2.87} + P_b \quad (2.6)$$

where P_{Xe} is the pressure corrected to Xe, P_{N_2} is the recorded pressure, P_b is the base pressure of the chamber and 2.87 is the correction factor between N_2 and Xe.

The next step toward finding the pumping speeds was to convert the flow rate data, measured in sccm, to throughput, measured in Torr-L/s. The conversion from flow rate to throughput is [41]:

$$Q(\text{Torr} - L/s) = \text{Flow Rate}(\text{sccm}) * \frac{760 \text{ Torr}}{1 \text{ std atm}} * \frac{1 \text{ L}}{1000 \text{ cm}^3} * \frac{1 \text{ min}}{60 \text{ s}} \quad (3.7)$$

The final pressure versus throughput data, as well as pressure versus flow rate data, recorded for the three pumps individually and combines are shown in Figures 2.9 and 2.10.

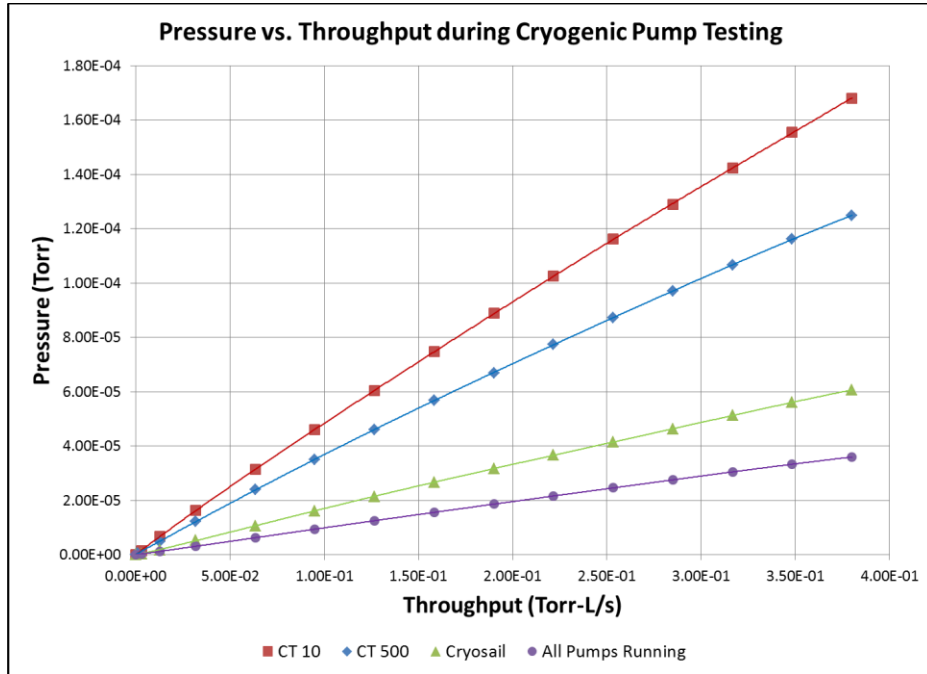


Figure 2.9. Results of pumping speed tests for cryogenic pumps.

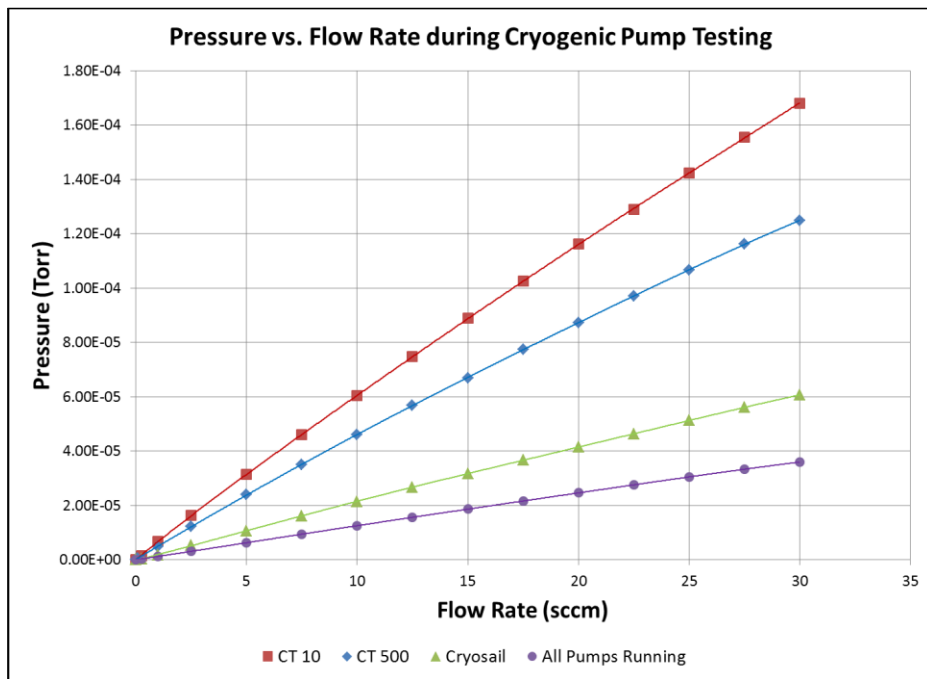


Figure 2.10. Results of pumping speed tests for cryogenic pumps.

The pump speed can be found from Figure 2.9 as the inverse of the slope of a linear fit line [41]:

$$P = \frac{Q}{S} \rightarrow \frac{dP}{dQ} = \frac{1}{S} \rightarrow \left(\frac{dP}{dQ}\right)^{-1} = S \quad (2.8)$$

The measured pumping speeds, found this way, are shown in Table 2.3.

Table 2.3. Summary of measured pumping speeds.

Cryogenic Pump	$S_{measured}$
CT 10	2,300 L/s
CT 500	3,000 L/s
Cryosail	6,200 L/s
Total	11,500 L/s
All Pumps Running	10,500 L/s

Although the same experimental techniques were used during all measurement experiments, a difference of 1,000 L/s between the summation of the individual pumping speeds and the measured pumping speed with all the pumps running was found. These two quantities are within 10% of each other; however, they should show better agreement. Their disagreement is probably caused by two factors. First, when all the pumps are running together, they probably influence the pumping speeds of each other. Since the chamber is in the scarce environment of molecular flow and the pumps are positioned opposite each other, they are somewhat in a competition to capture the remaining gas in the chamber. This may cause one or two of the pumps to have less efficient capture of the gas and contribute to the total pumping speed to be less than the sum of the individual pumping speeds.

Second, there is experimental uncertainty due to the drift and instability over time of the mass flow controllers used on the chamber. Since the pump speed tests were conducted at different times over a period of a couple weeks, small inconsistencies in flow settings of the mass flow controllers probably contributed to the mismatch. Additionally, it was later found that the pressure regulator on the Xe bottle caused oscillations in the flow to the mass flow controllers which in turn caused small fluctuations in the flow to the chamber most likely contributing to the difference between the two totals. Given the difference in totals, a value of

10,500 L/s provides a reasonable estimate of the total chamber pumping speed which is consistent with the goal of 8,000 L/s outlined in section 1.7.

2.6. Comparison of Estimated to Measured Pumping Speeds

Table 2.4 compares the estimated and measured pumping speeds of the HTECh's three cryogenic pumps. The measured pumping speed of the CT 10 is found to be over twice the estimated value. This discrepancy is attributed to the recent refurbishment of the pump as well as the very low conductance losses due to its position in the chamber as well as its flange geometry. The estimated pumping speeds of the CT 500 as well as the Cryosail matched well

Table 2.4. Comparison of estimated and measured pumping speeds.

Cryogenic Pump	S_{eff}	$S_{measured}$
CT 10	1,020 L/s	2,300 L/s
CT 500	3,000 L/s	3,000 L/s
Cryosail	6,840 L/s	6,200 L/s
Total	10,860 L/s	11,500 L/s

with their measured values. The adopted chamber pumping speed of 10,500 L/s matches well with the estimated total pumping speed of 10,860 L/s. Additionally, the chamber pressure with 30 sccm of Xe flowing was estimated at 3.5×10^{-5} Torr and measured at 3.6×10^{-5} Torr, thereby showing excellent agreement.

2.7. HTECh Conditions versus Space Conditions

The minimum required pumping speed of 8,000 L/s of Xe to operate a SPT-70 Hall thruster is achieved. The measured pumping speed with all pumps running was found as high as 11,500 L/s but a value of 10,500 L/s is adopted as the chamber's pumping speed. The required operating pressure of no higher than 5×10^{-5} Torr with flow of 30 sccm of Xe is met. The pressure with Xe flow was found as low as 3.6×10^{-5} Torr. The HTECh achieves the pumping

speed and pressure objectives (outlined at the beginning of this research effort) indicating it's a vacuum facility capable of testing and characterizing low power ($\lesssim 600$ W) Hall thrusters.

3.0 INITIAL TESTING OF A SPT-70 HALL THRUSTER

The Hall thruster operated in the HTECh is a SPT-70 developed and manufactured by the Experimental Design Bureau-Fakel located in Kaliningrad Oblast, Russia. This thruster is in the family of SPTs developed by the Russians and is slightly smaller than their most popular model, the SPT-100. The number designation of the model refers to the outer diameter, measured in millimeters, of the annular discharge channel [18]. The thruster operated in the HTECh was loaned to the CSU LPDL by the AFRL in support of our ongoing research efforts. In this chapter, installation and operation of the SPT-70 is described.

Figure 3.1 illustrates the SPT-70 and its cathode installed in the HTECh. The cathode's exit was positioned to be coincident at a magnetic separatrix as guided by past AFRL users to ensure electron availability to the discharge chamber.

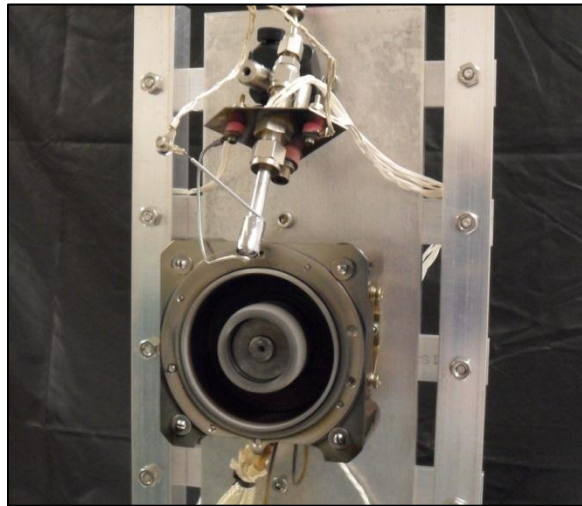


Figure 3.1. The SPT-70 and its cathode installed in the HTECh.

The positioning of the cathode is critical to proper operation of the thruster due to the important role electrons have in ionization and plume neutralization. In general, the cathode's exit orifice should be positioned just outside the discharge chamber and near the edge of the exhaust plume.

3.1. Installation and Supporting Equipment

Figure 3.2 illustrates a cutaway model of the chamber with the SPT-70 and a graphite target inside. As seen in the figure, the thruster is oriented horizontally at the end of the chamber with the cryogenic pump and faces the graphite target. A graphite target is placed in front of the cryosail to minimize thermal loading by the exhaust plume. The graphite target also minimizes the sputtering of the far chamber wall thus mitigating the amount of back sputtered wall material that could potentially redeposit on the thruster. The graphite target consists of eight fine grain graphite panels arranged to absorb the heat loading of the exhaust plume while providing gaps and offsets to only minimally affect the cryosail's pumping capabilities. The graphite material has a low sputter yield at the expected ion impact energies and therefore adds minimal particles to the chamber during thruster operation.

The thruster mounting stand that holds the thruster horizontally was designed to incorporate a vertical translation stage such that the thruster can be moved vertically during operation. This feature will later be used to move the thruster so that diagnostics and measurements can be conducted at different points in the plume. In Figure 3.2, the two flanges that lead to the CT 10 and CT 500 cryogenic pumps are labeled and the direction of the exhaust plume is indicated.

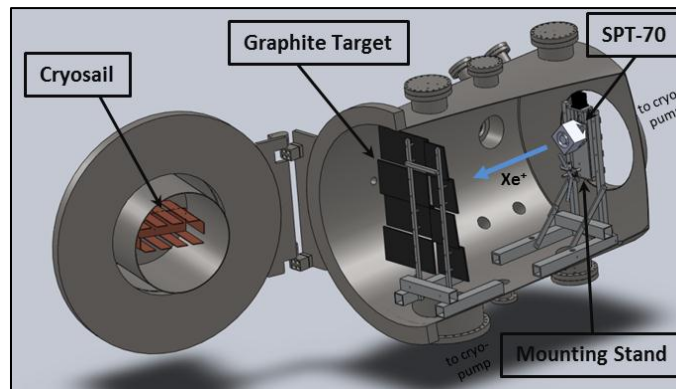


Figure 3.2. Cutaway drawing of the SPT-70 inside the HTECh.

Since a cathode was not included with the thruster when it was loaned to the university, one was built at CSU by another student (Lauren Rand) to meet our thruster testing needs. However, is not of an optimized design specific to the SPT-70. The cathode's operating principles are as described in section 1.1. Figure 3.3 illustrates the cathode used with the SPT-70. As seen in the figure, the cathode is constructed from Swagelok® fittings and tubing that

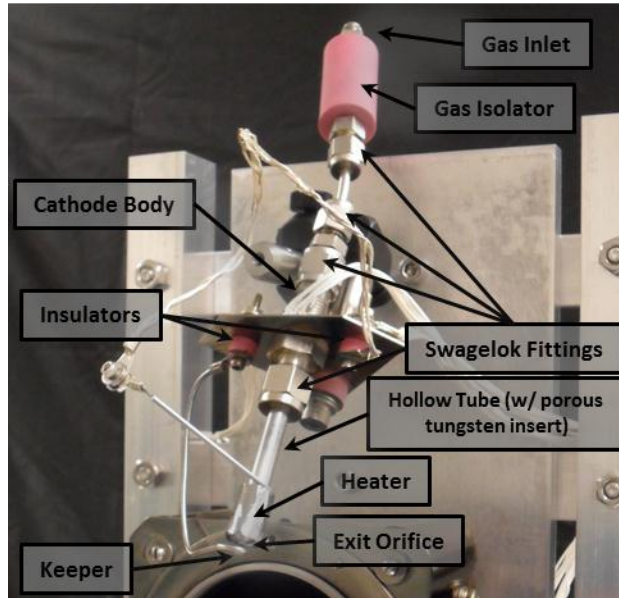


Figure 3.3. Cathode used with SPT-70.

connects the gas inlet thru an isolator to a hollow tube containing the insert. The cathode insert is made from porous tungsten impregnated with barium and is surrounded by the heater. The keeper ends in a small loop and is placed approximately 0.05 in from the exit orifice. During operation, the keeper is biased around 14 V to contain plasma inside the hollow tube while allowing electrons to exit. Ceramic insulators are used such that the cathode's body, heater and keeper are all electrically isolated from each other as well as from chamber ground. There is a specific time sequenced start-up procedure used to operate the cathode included as Appendix A to this thesis. The start-up procedure was specified by the student who built it and must be

followed to purge the cathode of contaminants prior to operation. Improper start-up will limit the life of the cathode.

The required equipment to power and fuel the SPT-70 and its cathode includes four power supplies and two mass flow controllers. The cathode requires two power supplies, one for its heater and one for its keeper. The thruster requires two power supplies, one for its anode and one for its magnets. Additionally, both the cathode and the thruster each require a mass flow controller. Table 3.1 shows the details of the equipment used to operate the thruster and its cathode. Appendix B provides the system’s wiring diagram as well as the thruster start-up procedure.

Table 3.1. Supply components for the SPT-70.

Component	Component Specification
Cathode Heater Power Supply	80 V, 13 A DC Supply
Cathode Keeper Power Supply	600 V, 1.7 A DC Supply
Cathode Mass Flow Controller	5-50 sccm, 500 psi max.
Thruster Anode Power Supply	330 V, 10 A DC Supply
Thruster Magnets Power Supply	50 V, 5 A DC Supply
Thruster Mass Flow Controller	5-50 sccm, 500 psi max.

3.2. Expected Operating Conditions

Table 3.2 outlines the operating conditions of three Hall thrusters of interest. The BHT-600 manufactured by Busek is a thruster similar to the SPT-70. As seen in the table, the BHT-600’s discharge voltage and current produces similar thrust and I_{sp} to the SPT-70.

Table 3.2. Thruster characteristics of small Hall thrusters [18].

Thruster Type	Thrust	I_{sp}	$\eta_{thruster}$	\dot{m}_{Xe}	$P_{discharge}$	$V_{discharge}$	$I_{discharge}$
SPT-70	40 mN	1510 s	46%	2.35 mg/s	600 W	300 V	2.1 A
BHT-600	41 mN	1600 s	52.5%	2.6 mg/s	600 W	300 V	2.05 A
SPT-100	83 mN	1600 s	48%	5.5 mg/s	1350 W	300 V	4.5 A

The SPT-100 is the next larger thruster in Fakel's family of Hall thrusters and is included for comparison purposes. As seen in the table, the discharge voltage, I_{sp} and efficiency are similar to the SPT-70. However, the mass flow rate and discharge current and resulting thrust are approximately two times that of the SPT-70.

An interesting feature of the SPT-70 is the ability to independently control the amount of current to the magnets. This is a unique feature that not all thrusters possess. Typically, the anode current, commonly referred to as the discharge current, and the magnet current are approximately the same [42]. In fact, some thrusters have the magnets and the anode connected in series such that the current is always the same. However, having the ability to adjust the current to the magnets independently is advantageous because it allows fine tuning of the magnetic field which in turn leads to the highest thruster efficiency.

The highest thruster efficiency is found at the magnet current that minimizes the discharge current (and maximizes the channel impedance) [43]. This operating point physically corresponds to the most efficient use of electrons to ionize the propellant. If the current to the magnets is adjusted above the most efficient point, electrons in the discharge chamber start to create multiply charged ions resulting in an excess of electrons that cause the discharge current to increase. If the current to the magnets is adjusted below the most efficient point, some electrons escape the circular magnetic field inside the discharge chamber without ionizing any propellant and cause the discharge current to increase.

3.3. SPT-70 Operation

The SPT-70 and its cathode were operated in the HTECh. Two pictures of the thruster and its cathode operating using Xe as the propellant are illustrated in Figure 3.4. As seen in the figure, the tip of the cathode is glowing orange indicative of proper heating and electron

production. The neon-blue colored plume seen in the figure is indicative of proper propellant ionization.

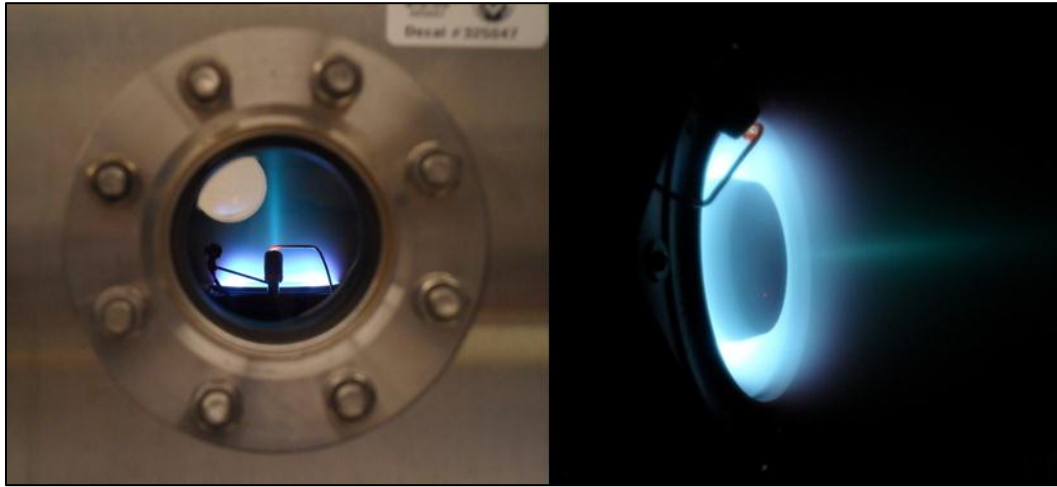


Figure 3.4. SPT-70 operating on Xe in the HTECh.

During operation, the pressure is monitored in the HTECh to ensure it remains no higher than 5×10^{-5} Torr. The cathode heater current and cathode flow rate are reduced as much as possible to minimize the heat and mass loads on the cryogenic pumps. As stated in section 3.2, to find the most efficient thruster operating point, the current to the magnets is tuned to minimize the discharge current. Figure 3.4 illustrates the results of a test to find the minimum discharge current. During testing of the SPT-70 in the HTECh, a minimum discharge current was found to be approximately 1.5 A. The minimum discharge current occurs when the magnet current is approximately 2.5 A. A distinct minimum is seen in the graph corresponding to the most efficient point of thruster operation. Magnet currents above 2.7 A were not investigated further due to concerns of overheating the magnets. Potential overheating was indicated by the discharge channel glowing red after thruster operations ceased.

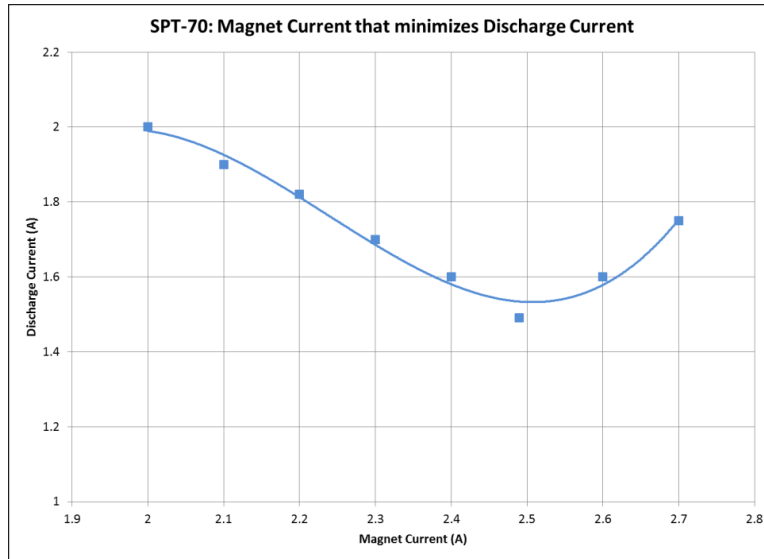


Figure 3.4. Minimization of discharge current as magnet current varied.

The SPT-70 and its cathode operated in the HTECh at vacuum conditions similar to conditions at other research facilities. Although the total pumping speed of the HTECh is much lower than other thruster testing facilities, the ability to keep high vacuum around 5×10^{-5} Torr during thruster operation validates the HTECh as a facility capable of producing accurate performance measurements. The overall pumping speed of the system was reduced when the graphite target was placed in the chamber due to the conductance losses introduced. The target's graphite panels restrict molecular flow to the cryosail such that the total pumping speed of the chamber is reduced to around 7,400 L/s. A future iteration of the graphite target design should include a closed loop liquid nitrogen system to cool the graphite panels to cryogenic temperatures. Future target designs to mitigate conductance losses should also be investigated. Additionally, the addition of a turbo molecular pump to the HTECh could add up to 600 L/s of pumping capacity. With these modifications, the chamber will better meet the pressure and pumping speed requirements for SPT-70 operation.

3.4. Faraday Probe Measurements

Measurements of ion current densities in the plasma plume of the SPT-70 were performed to obtain more detailed understanding of thruster operation. A Faraday probe is a diagnostic instrument used to measure the ion current density in the far field plume of a thruster. There are several types of Faraday probes including nude, cupped, collimated, gridded and magnetically filtered. A standard Faraday probe, known as a nude probe, is biased below the plasma potential to ensure that plasma electrons are repelled and only ions are collected. Ions impacting the probe create a measurable current that is used to find the ion current density at various positions in the plume [44].

One of the challenges encountered when using a Faraday probe is that charge exchange ions can be attracted to the probe due to its negative bias. Charge exchange ions are low-energy ions resulting from charged particles colliding with neutral background gases. The number of charge exchange ions increase with increasing chamber pressure. Charge exchange ions artificially inflate the measured ion current density. A collimated probe is often used to limit the collection of charge exchange ions and more accurately measure the current density in the plume of a thruster. A collimated Faraday probe is very similar to the nude probe except that the probe has a cover with a small aperture leading to the collection surface. When pointed at the thruster's exit plane, the aperture only allows ions with a narrow range of velocity vectors to reach the collecting surface thus acting as a filter for the charge exchange ions travelling in random directions [44]. Figure 3.5 shows the nude and collimated Faraday probes used for plasma measurements in the HTECh.



Figure 3.5. Faraday probes used for plasma measurements.

Figure 3.6 illustrates the electrical circuitry and power supplies needed to operate the Faraday probe used for plasma measurements in the HTECh. The probe body and collector plate are electrically insulated from one another such that various biasing schemes can be used to collect ions from the plume. The probe in Figure 3.6 is in a collimated configuration noted by

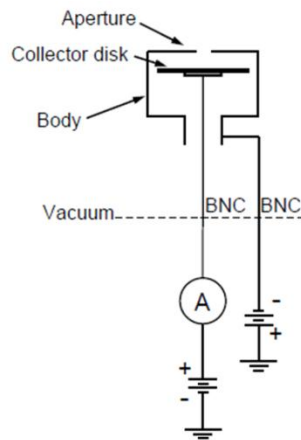


Figure 3.6. Electrical schematic of a Faraday probe.

the aperture in front of the collector disk. In this configuration, the body of the probe is biased negative to repel electrons while the collector disk is biased positive to eliminate collection of charge exchange ions. The aperture allows collection of ions from the plume arriving perpendicular to the probe face.

The surface area of the collector in the nude configuration is 0.5 cm^2 , much larger than the collimated probes surface area of 0.01 cm^2 . Given the larger collector area, if the nude collecting surface is biased positive, it will attract electrons even when the probe's body is biased negative due to the probe's shape and geometry. In this case, the probe is unable to measure ions. Therefore, when the probe is used in a nude configuration, both the body and the collector are biased negative to repel electrons and attract ions.

The results of a Faraday probe measurement series is illustrated in the left graph of Figure 3.7. The ion current measurements shown in the figure are representative of typical results. A nude probe configuration was used with -20 V and -30 V biases on the body and collector, respectively. These were the biases recommended for use by the probe's manufacturer (Plasma Controls, LLC). The probe was placed 50 cm downstream of the thruster exit plane and measurements were taken every centimeter from the thruster centerline outward to 23 cm such that the probe face was always parallel to the thrusters exit plane. In probe measurements done by other researchers, the probe geometry is such that the probe travels on a radius downstream of the thruster such that the probe face is always aiming toward the thruster's exit plane. Because the interest was in preliminary ion density results, a simple apparatus to move the probe only linearly was constructed and used for measurements. A more complex apparatus to do measurements at constant radial distances downstream of the thruster is the next evolution for the HTECh.

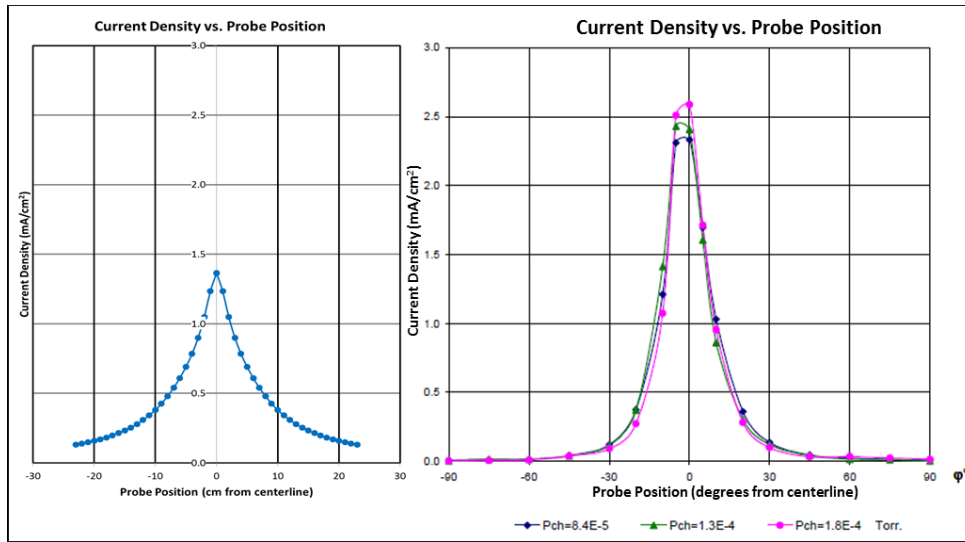


Figure 3.7. Faraday probe measurements of a SPT-70 during operation.

In Figure 3.7, measurement symmetry about the thruster centerline is assumed and therefore (mirrored) current densities from 0 to -23 cm were added for comparison to results from Kim et al. [42] seen in the right graph. The measurements from Kim were taken when their thruster was operating at 300 V and 2 A of discharge voltage and current, respectively and an anode flow rate of 24 sccm. Their probe was also located 50 cm downstream of the thruster exit plane and, as seen by their legend, evaluated at three different background pressures.

When comparing the graphs, it is obvious that the results from testing the SPT-70 in the HTECh are less than the results from Kim. The maximum measured current density was found to be 1.4 mA/cm^2 while the maximum measurement made by Kim is 2.6 mA/cm^2 . When the measurements from the HTECh are integrated, a total beam current of 0.66 A is found while an integration of Kim's data results in a total beam current of 1.7 A.

The difference between these two results is most likely due to the lower anode flow rate of the thruster operated in the HTECh. It is expected that for every 14 sccm of Xe flowing through the anode, the thruster will produce 1 A of beam current. In fact, Beam current (J_{beam}) is found using [6]:

$$J_{beam} = \frac{\dot{m}_{ion} \cdot q}{M_{ion}} \quad (3.1)$$

where \dot{m}_{ion} is ion mass flow rate, q is the ion charge and M_{ion} is the ion mass. The beam current estimation stated above assumes that all Xe atoms are ionized and they are all singly charged. The thruster tested in the HTECh had an anode flow of 13.5 sccm which, according to Equation 3.1, should correspond to 0.97 A of beam current, however, the results showed it was 0.66 A. Kim's thruster had a flow rate of 24 sccm which corresponds to 1.7 A of beam current. Kim's calculated and measured beam currents are the same.

3.5. Thruster Operation Issues

Nominal conditions for the SPT-70 include an anode voltage, current and flow rate of 300 V, 2.2 A and 24 sccm, respectively. During operation of the SPT-70 in the HTECh, attaining nominal conditions was a challenge. As the anode flow rate was increased past 13.5 sccm, the anode voltage would not exceed 90 V. The anode voltage remained low even as the magnet current was increased to around 2.5 A. Magnet current exceeding 2.5 A was not tested due to potential damage to the thruster.

Troubleshooting the thruster issues included adjusting the cathode position and flow rate, adjusting the graphite target to reduce the conductance losses and increase the chamber's pumping speed and adding a reservoir to the propellant supply system to mitigate flow oscillations and inaccuracies in the mass flow controllers. Despite these steps, nominal operation was not achieved and the beam current, as described in the previous section, remained lower than expected.

The thruster's discharge current was also very sensitive to small adjustments to the magnet current and adjustments extinguished the plasma on many occasions. It was decided to investigate the magnetic field of the thruster in order to verify that it's within design

specification. The thruster was sent to the NASA Glenn Research Center and the thruster's magnetic field was mapped. The feedback received indicates that the peak magnetic field along the channel centerline is low (90 Gauss) when the magnets were supplied with 2.5 A. The peak along the centerline of the magnetic field should be approximately 120 Gauss [45]. The weak magnetic field does not provide the proper Hall effect to the thruster allowing electrons to reach the anode at higher rates than normal, indicated by a high discharge current. Additionally, the electrons can reach the anode without ionizing any propellant, causing a low beam current.

The weak magnetic field is most likely caused by magnet degradation or damage due to age or misuse. The wire in the coil could be damaged and short circuiting when power is applied. The use history of the SPT-70 is not available and disassembly for further troubleshooting is not currently an option. Efforts to secure another low power Hall thruster for additional testing and operation are ongoing.

4.0 SPUTTER EROSION STUDY BY CRDS

One of the motivations for developing the HTECh is to perform laser-based studies of erosion using Cavity Ring-Down Spectroscopy (CRDS). While the CRDS effort is led by another student (Brian Lee), initial results are presented here to demonstrate the suitability of the HTECh for CRDS. In this chapter, a brief overview of CRDS is discussed and preliminary CRDS measurement results are presented.

4.1. CRDS Technique Overview

The sputter yield of thruster wall material is generally low and therefore difficult to measure even with very sensitive instruments. CRDS is a laser measurement technique with sufficient sensitivity to measure the amount of Boron sputtered from the thruster walls [46–48]. CRDS is an absorption technique where a sample volume of the thruster's exhaust plume is probed with a laser. Laser wavelengths around 250 nm are used for probing because light at these wavelengths correspond to resonance lines of neutral Boron. Two high-reflectivity mirrors ($R \sim 0.998$) separated by a set distance create an optical cavity to sample a volume of the thruster's exhaust plume to measure Boron. Light from a continuous wave laser is reflected between the mirrors and only a fraction of the light leaves the cavity each time it is reflected. The high-reflectivity mirrors allow the light to make thousands of passes in the cavity before its intensity diminishes. These passes create a long effective path length resulting in the ability to take highly sensitive measurements of Boron [46].

During each pass, a small portion of light escapes the cavity through the output mirror. A detector is positioned to measure the optical intensity of the escaped light. The decay rate of the measured optical intensity is termed the ring-down time and given the symbol τ . The difference in the ring-down time with and without Boron (the absorber) present yields the concentration of

Boron [46]. A basic diagram of a CRDS set-up as well as sample detector outputs are illustrated in Figure 4.1. As seen in the figure, the signal intensity decays exponentially with time.

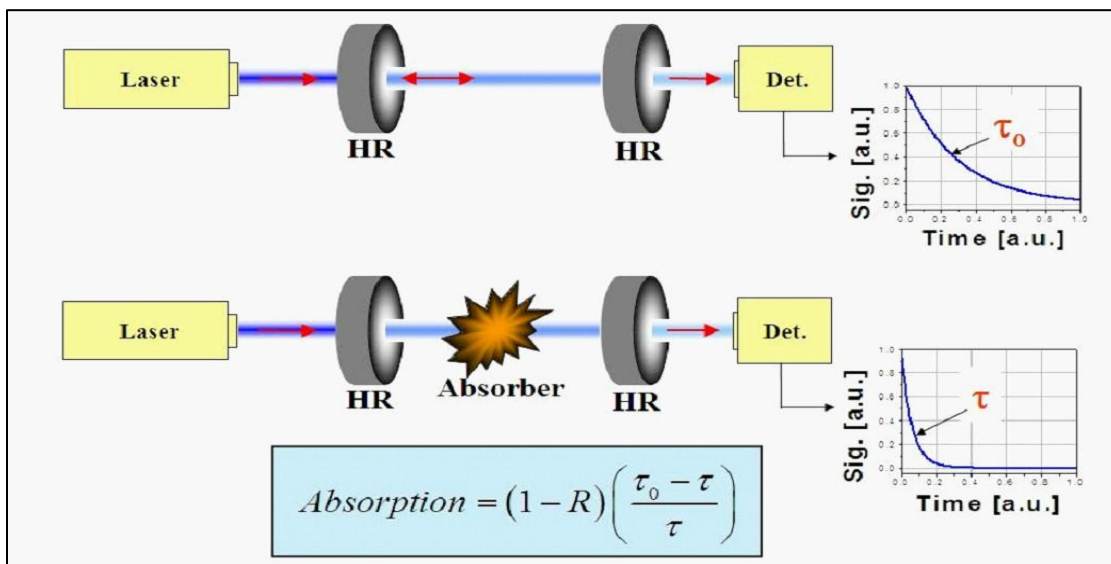


Figure 4.1. Basic diagram of CRDS [46].

During CRDS measurements, a fast photomultiplier tube detector measures the optical intensity and passes those measurements to a computer program that records the data as a function of time. The program fits the raw data with an exponential and a ring-down time is extracted using [46]:

$$S(t, \nu) = S_0 \cdot \exp \left[\frac{-t}{\tau(\nu)} \right] \quad (4.1)$$

where $S(t, \nu)$ is the recorded signal intensity as a function of time and laser frequency (ν), S_0 is the initial signal intensity and $\tau(\nu)$ is the ring-down time.

As seen in Equation 4.1, signal intensity and ring-down time are both functions of laser frequency. When using CRDS to measure concentrations of Boron, the laser's wavelength is scanned across a small range of wavelengths near the known Boron absorption line of 249.848 nm. When the laser's wavelength reaches the absorption line, Boron in the sample volume causes the ring-down time to decrease sharply. The ring-down time versus wavelength data is

used to determine the absorbance spectrum. The left panel of Figure 4.2 displays ring-down times as the laser is scanned over wavelengths near a Boron absorption line. The right panel of Figure 4.2 displays the corresponding absorbance spectrum for Boron. Both plots indicate the presence of Boron in the optical cavity.

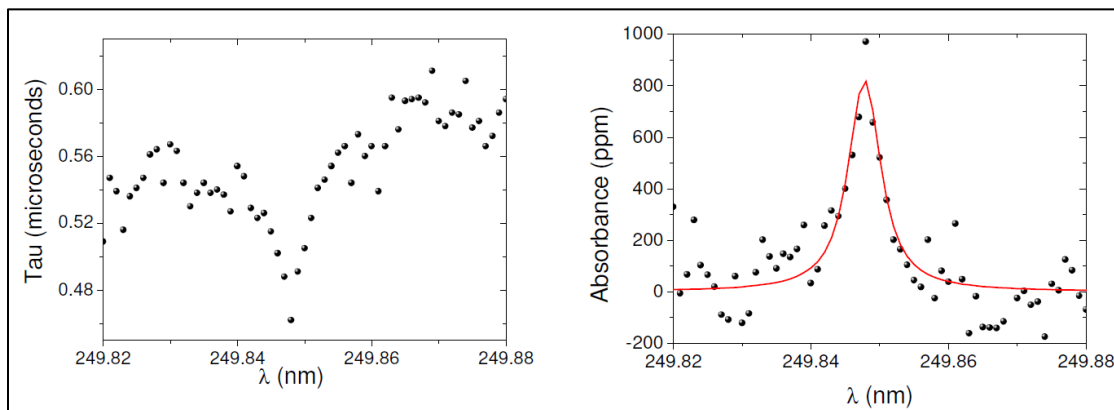


Figure 4.2. Plots of ring-down time and absorbance for Boron [46].

Although the exact composition of sputtered wall material is not known, it is assumed that the wall material sputters in equal parts and the sputtered material composition represents the wall material composition. This assumption allows quantitative measurements of Boron from the wall material to be found from the analysis of the absorbance spectrum [46].

4.2. Preliminary CRDS Results

A CRDS system to study the sputtered Boron products in the plume of the SPT-70 Hall thruster was installed in the HTECh. A Toptica frequency quadrupled tunable diode laser was used to create light at approximately 250 nm for absorption measurements. The laser, steering mirrors and alignment optics were set on an optical table next to the chamber. The laser enters the chamber through an ultraviolet grade fused silica window. It then encounters a 54 cm optical cavity created using two high-reflectivity mirrors. The optical cavity is set across the centerline of the SPT-70 at its exit plane. A fiber optic cable is attached to the output mirror and feeds the

light that escapes the optical cavity to a fast photomultiplier. The signal from the fast photomultiplier is used to determine ring-down times.

Figure 4.3 illustrates the SPT-70 mounted in the chamber with the optical components mounted to a support frame surrounding the thruster. As seen in the figure, the optical cavity is

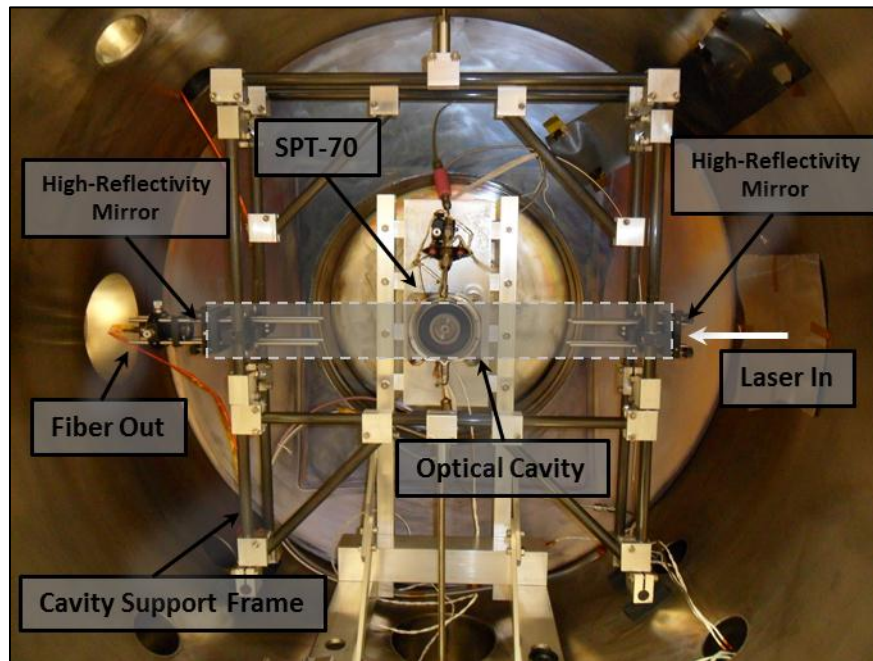


Figure 4.3. The SPT-70 and CRDS components mounted inside the HTECh.

across the centerline of the thruster. The highlighted area in the figure is much larger than the actual optical cavity. The optical cavity is 54 cm long; however, it is only as tall as the diameter of the laser beam (~2 mm). Both mirror mounts are attached to aligning fixtures which are in turn attached to the cavity support frame. The cavity support frame is made from a composite material with a low coefficient of thermal expansion. The cavity support frame is attached to the chamber at two points by threaded stainless steel rods into two modified chamber flanges. Additionally, the cavity support frame sits on vacuum safe rubber feet to dampen any vibration from the chamber's supporting equipment. The cavity support frame is constructed in this way

so that it easily maintains its alignment during temperature and pressure changes as well as from vibration encountered during chamber operations.

Using the set-up described above, CRDS measurements were taken when the thruster was in operation at an approximate discharge voltage and current of 300 V and 2 A, respectively.

Figure 4.4 shows the results of the initial CRDS measurements.

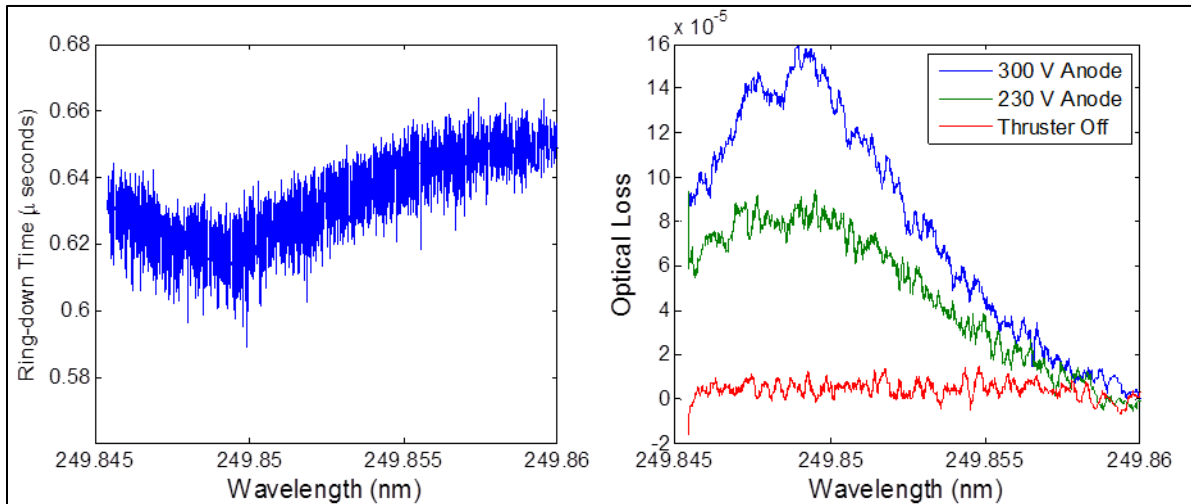


Figure 4.4. Initial CRDS measurement results of SPT-70 in HTECh.

The left panel of Figure 4.4 illustrates how the ring-down time reaches a minimum over a small range of laser wavelengths. This minimum indicates that laser light at approximately 249.85 nm is being absorbed in the optical cavity. As discussed, Boron has an absorption line at a laser wavelength of 249.848 nm. The right panel of Figure 4.4 illustrates the loss in the optical cavity. Optical losses were measured with the thruster off and then again with anode voltages of 230 V and 300 V. As seen in the figure, optical loss is higher for the 300 V operating point as compared to the 230 V operating point. This occurs because there are more sputtered Boron products in the plume of the thruster at this higher operating voltage. The initial results presented here indicate that Boron is being detected in the thruster plume and measurements using CRDS are possible in the HTECh facility.

5.0 CONCLUSION

The goal of this research effort was to assemble a chamber and supporting equipment to operate a SPT-70 Hall thruster at chamber pressures that provided sufficient conditions for accurate performance measurements. After extensive chamber, equipment and facility renovations and refurbishments, a SPT-70 was operated in the HTECh. It is concluded that the HTECh is capable of creating sufficient high vacuum conditions that allow successful diagnostic tests of a low power Hall thruster.

The literature review to support the research included Hall thruster component functions and characteristics as well as Hall thruster fundamental operating principles. The governing equations such as the Lorentz Force Law were summarized. Additionally, the history and current uses of Hall thrusters were examined. It was found that the popularity of Hall thrusters for satellite station keeping and long duration missions is increasing owing to their increased specific impulse over chemical thrusters. In fact, Hall thrusters are found on many commercial satellites and recently have made their first appearance on an Air Force communications satellite constellation. It is expected that Hall thrusters will continue to be used by a variety of satellite owners so understanding their operating parameters will remain an important research need.

The refurbishment and assembly of the HTECh required significant labor to complete but was made possible by the donation of a LADS chamber from the AFRL as well as two cryogenic pumps from a local business. One of the highlights of the refurbishment process was the rebuilding of the three cryogenic pump cold heads. While this task is usually done by the manufacturer, it was decided to do this in-house in order to get a better understanding of cryogenic pump operation. The knowledge acquired from the rebuild process helped in the

design and construction of custom cryogenic pump stages that were incorporated in the HTECh, referred to as the cryosail.

The estimated as well as measured cryogenic pumping speeds were presented for the CT 10, CT 500 and cryosail attached to the chamber. Estimated pumping speeds were found from published pumping speed data and estimated conductance losses due to the pumps' flanges. A similar estimation was done for the cryosail and then all three effective pumping speeds were summed to get the total pumping speed of the chamber. The total pumping speed of the system was estimated around 10,860 L/s of Xe. The measured pumping speed was found by flowing Xe into the chamber at increasing flow rates while recording the pressure. Measurements were made for each pump individually as well as all three pumps running together. The measurements were then analyzed to determine the total measured pumping speed. The total pumping speed of the system was found to be 10,500 L/s of Xe in good agreement with the estimate.

It was found that the majority of the pumping speed capability of the system came from the custom built cryosail. While the cryosail pumping speed was estimated at 6,840 L/s of Xe, its measured pumping speed was only 6,200 L/s. The difference is most likely due to unaccounted conductance losses during operation. However, this is still an impressive capability from a relatively simple device which is instrumental in creating the high vacuum necessary to operate the SPT-70.

The SPT-70 operated in the HTECh was of Russian origins and was loaned to the university by the AFRL. A cathode built in-house was used with the SPT-70. While relatively simple in operation, it was found that the cathode is delicate and subject to oxidation if exposed to air while at operating temperature. Recommended warm-up and cool down procedures were

followed to mitigate this issue. Various discharge voltages and currents were examined and the thruster was operated at its maximum setting of 600 W of discharge power.

During testing, the thruster was mounted at one end of the chamber in such a way that its plume could be examined and measured. A graphite target was placed downstream of the thruster in order to reduce unwanted sputtering of chamber components and reduce the heat load on the cryosail. However, the overall pumping speed of the system was reduced when the graphite target was placed in the chamber. The target's graphite panels restrict molecular flow to the cryosail such that the total pumping speed of the chamber was reduced to 7,350 L/s.

Testing to understand the ion current in the plume of the SPT-70 was done using a nude Faraday probe placed downstream of the exit plane. These tests captured spatially resolved current density measurements and their results were integrated to find the current downstream of the thruster. The current found was lower than anticipated probably due to low propellant ionization caused by a degraded magnetic field.

Investigation into the magnet field in the SPT-70 resulted in the discovery that the peak magnetic field along the channel centerline is lower than desired. A magnetic field strength of 90 Gauss was measured whereas the peak strength should be around 120 Gauss. The degraded magnetic field probably contributed to the thruster's inability to reach nominal operating conditions.

Spacecraft utilizing Hall thrusters must be able to operate them for over ten thousand hours in order to meet mission requirements [32]. Testing Hall thrusters for thousands of hours is very difficult and expensive. Specifically, sputtering of the thruster's wall material by energetic ions over the thruster's lifetime is difficult to understand. However, during this research effort, preliminary CRDS was conducted to determine if this laser measurement

technique had the capability and sensitivity to measure sputtered Boron products in the plume of the SPT-70. The results of initial testing indicate that the CRDS set-up used with the HTECh allowed in situ erosion measurements. This non-invasive technique has the capability to produce sputter measurements necessary to better estimate factors involved in the codes of thruster computer models. Since thruster characteristics can change after channel wall erosion and sputtered products can degrade or damage other spacecraft systems, an understanding of their lifetimes is advantageous to spacecraft designers.

6.0 REFERENCES

- [1] S. Y. Cheng, “Modeling of Hall Thruster Lifetime and Erosion Mechanisms,” Massachusetts Institute of Technology, 2007.
- [2] A. Smirnov, Y. Raitses, and N. J. Fisch, “Experimental and Theoretical Studies of Cylindrical Hall Thrusters,” *Physics of Plasmas*, vol. 14, no. 5, p. 057106, 2007.
- [3] A. Vesselovzorov, D. Grdlichko, and V. Kim, “Study of the Accelerating Channel Wall Property Influence on the Hall Thruster Discharge Characteristics,” Moscow, Russia, 2004.
- [4] W. Camperchiolo, “Thermal Vacuum Testing Vacuum Facility 5 at NASA Glenn Research Center,” Cleveland, 2011.
- [5] R. Hofer, “Characterizing Vacuum Facility Backpressure Effects on the Performance of a Hall Thruster,” *27th International Electric Propulsion Conference*, no. IEPC-01-045, 2001.
- [6] D. Goebel and I. Katz, *Fundamentals of Electric Propulsion: Ion and Hall Thrusters*, 1st ed. Pasadena: California Institute of Technology, 2008, p. 486.
- [7] E. Y. Choueiri, “Fundamental Difference Between the Two Hall Thruster Variants,” *Physics of Plasmas*, vol. 8, no. 11, p. 5025, 2001.
- [8] N. Fisch and J. Choi, “What’s a Hall Thruster?,” 2008. [Online]. Available: <http://htx.pppl.gov/ht.html>. [Accessed: 07-Aug-2012].
- [9] R. Hofer, “High-Specific Impulse Hall Thrusters, Part 1: Influence of Current Density and Magnetic Field,” *Journal of Propulsion and Power*, vol. 22, no. 4, pp. 721–731, 2006.
- [10] S. Mazouffre, K. Dannenmayer, and J. Pérez-Luna, “Examination of Plasma-Wall Interactions in Hall Effect Thrusters by means of Calibrated Thermal Imaging,” *Journal of Applied Physics*, vol. 102, no. 2, p. 023304, 2007.
- [11] R. Hofer, “Development and Characterization of High-Efficiency, High-Specific Impulse Xenon Hall Thrusters,” Ann Arbor, MI, 2004.
- [12] J. Rotter, “An Analysis of Multiple Configurations of Next-Generation Cathodes in a Low Power Hall Thruster,” Air Force Institute of Technology, 2009.
- [13] O. Lapy and A. Menard, “Satellite Propulsion - Snecma,” 2012. [Online]. Available: <http://www.snecma.com/-satellite-propulsion-.html?lang=en>. [Accessed: 07-Aug-2012].

- [14] S. Oleson, "Advanced Hall Electric Propulsion for Future In-Space Transportation," *Third International Spacecraft Propulsion Conference*, no. NASA/TM-2001-210676, 2001.
- [15] M. Dudeck and F. Doveil, "Plasma Propulsion for Geostationary Satellites and Interplanetary Spacecraft," *Journal of Applied Physics*, vol. 56, no. July 2010, pp. 3-14, 2011.
- [16] J. Sellers, *Understanding Space: An Introduction to Astronautics*, 3rd ed. New York: , 2000, p. 774.
- [17] V. Kim, "History of the Hall Thrusters Development in USSR," *30th International Electric Propulsion Conference*, no. IEPC-2007-142, 2007.
- [18] C. Clauss and D. Tilley, "Benefits of Low-Power Stationary Plasma Thruster Propulsion for Small Satellites," Gainesville, VA, 1995.
- [19] S. Daily, "The First US Hall Thruster Is Operational In Space," 2007. [Online]. Available: http://www.space-travel.com/reports/The_First_US_Hall_Thruster_Is_Operational_In_Space_999.html. [Accessed: 07-Aug-2012].
- [20] A. Mathers, K. D. Grys, and J. Paisley, "Performance Variation in BPT-4000 Hall Thrusters," *31st International Electric Propulsion Conference*, no. IEPC-2009-144, 2009.
- [21] S. Daily, "Aerojet's High-Power Hall System Propels USAF AEHF Satellite," 2010. [Online]. Available: http://www.space-travel.com/reports/Aerojet_High_Power_Hall_System_Propels_USAF_AEHF_Satellite_999.html. [Accessed: 07-Aug-2012].
- [22] D. Nox, "Space Vids," 2012. [Online]. Available: <http://spacevids.info/index.php/atlas-v-aehf-2/>. [Accessed: 22-Aug-2012].
- [23] Saint-Gobain, "Boron Nitride Products," 2012. [Online]. Available: http://www.bn.saint-gobain.com/news_detail.aspx?id=255700. [Accessed: 07-Aug-2012].
- [24] J. T. Yim, M. Keidar, and I. D. Boyd, "An Investigation of Factors Involved in Hall Thruster Wall Erosion Modeling," *42nd AIAA/ASME/SAE/ASEE Joint Propulsion Conference and Exhibit*, no. AIAA-2006-4657, 2006.
- [25] O. Duchemin, J. Brophy, and C. Garner, "A Review of Low Energy Sputtering Theory and Experiments," Pasadena, CA, 1997.
- [26] O. Duchemin, "An Investigation of Ion Engine Erosion by Low Energy Sputtering," California Institute of Technology, Pasadena, CA, 2001.

- [27] S. Khartov, "SPT's High Lifetime – Some Problems of Solution," *29th International Electric Propulsion Conference*, no. IEPC-2005–62, 2005.
- [28] Y. Garnier, V. Viel, J. Roussel, and J. Bernard, "Low-Energy Xenon Ion Sputtering of Ceramics Investigated for Stationary Plasma Thrusters," *Journal of Vacuum Science & Technology A: Vacuum, Surfaces, and Films*, vol. 17, no. 6, p. 3246, 1999.
- [29] B. Rubin, J. L. Topper, and A. P. Yalin, "Total and Differential Sputter Yields of Boron Nitride Measured by Quartz Crystal Microbalance," *Journal of Physics D: Applied Physics*, vol. 42, no. 20, p. 205205, 2009.
- [30] V. Abgaryan, H. Kaufman, and V. Kim, "Calculation Analysis of the Erosion of the Discharge Chamber Walls and their Contamination during Prolonged SPT Operation," *30th AIAA/ASME/SAE/ASEE Joint Propulsion Conference and Exhibit*, no. AIAA 94–2859, 1994.
- [31] A. Shagayda, O. Gorshkov, and D. Tomilin, "The Effect of Wall Erosion on the Performance of Hall Thrusters," *32nd International Electric Propulsion Conference*, no. IEPC-2011–025, 2011.
- [32] T. Randolph and V. Kim, "Facility Effects on Stationary Plasma Thruster Testing," *23rd International Electric Propulsion Conference*, no. IEPC-93–093, 1993.
- [33] H. T. Corporation, "Cryo-Torr @ Pump Installation , Operation and Maintenance Instructions," Mansfield, MA, 2005.
- [34] M. Thirumaleshwar and R. M. Pandey, "Two Stage Gifford-McMahon Cycle Cryorefrigerator Operated by Gas Balancing Principle," *Cryogenics*, vol. 30, no. 2, pp. 100–104, Feb. 1990.
- [35] M. A. T. E. Center, "Cryogenic Pump Theory of Operation." [Online]. Available: <http://matec.org/ps/library3/secure/modules/100/LA3/M100LA3.html>. [Accessed: 08-Aug-2012].
- [36] R. P. Institute, "Adsorption," 2000. [Online]. Available: <http://www.rpi.edu/dept/chem-eng/Biotech-Environ/Adsorb/adsorb.htm>. [Accessed: 08-Aug-2012].
- [37] J. F. Peterson and H. A. Steinherz, "Vacuum Pump Technology; A Short Course on Theory and Operations," *Solid State Technology*, Waltham, MA, 1982.
- [38] N. Marquardt, "Introduction to the Principles of Vacuum Physics," University of Dortmund, Dortmund, Germany, 1999.
- [39] R. Rutledge, *Practical Vacuum Systems*. New York: McGraw-Hill Book Co., 1987, pp. 73–77.

- [40] J. Moore and M. Coplan, *Building Scientific Apparatus*. Cambridge: Cambridge University Press, 2002, p. 654.
- [41] P. Wilbur, “MECH 567-Broad Beam Ion Sources,” Colorado State University, Fort Collins, CO, 2009.
- [42] V. Kim, V. Kozlov, and G. Popov, “Plasma Parameter Distribution Determination in SPT-70 Plume,” *28th International Electric Propulsion Conference*, no. IEPC-2003–007, 2003.
- [43] V. Kim, “Main Physical Features and Processes Determining the Performance of Stationary Plasma Thrusters,” *Journal of Propulsion and Power*, vol. 14, no. 5, pp. 736–743, Sep. 1998.
- [44] R. Hofer, M. Walker, and A. D. Gallimore, “A Comparison of Nude and Collimated Faraday Probes for Use with Hall Thrusters,” *27th International Electric Propulsion Conference*, no. IEPC-01–020, 2001.
- [45] A. Vesselovzorov, A. Pogorelov, E. Svirskiy, and V. Smirnov, “Low Frequency Wave Experimental Investigations, Transport and Heating of Electrons in Stationary Plasma Thruster,” *32nd International Electric Propulsion Conference*, no. IEPC-2011–060, 2011.
- [46] A. Yalin, L. Tao, N. Yamamoto, T. Smith, and A. Gallimore, “Boron Nitride Sputter Erosion Measurements by Cavity Ring-Down Spectroscopy,” *30th International Electric Propulsion Conference*, no. IEPC-2007–075, 2007.
- [47] W. Huang, A. Gallimore, T. Smith, L. Tao, and A. Yalin, “Initial Cavity Ring-Down Density Measurement on a 6-kW Hall Thruster,” *47th AIAA/ASME/SAE/ASEE Joint Propulsion Conference & Exhibit*, no. AIAA 2011–5994, 2011.
- [48] B. Lee, L. Tao, J. Taylor, and A. Yalin, “Sensitivity Improvements to Laser Sensor for Boron Nitride Erosion in Hall Thrusters,” *32nd International Electric Propulsion Conference*, no. IEPC-2011–068, 2011.
- [49] V. Murashko and A. Koryakin, “Russian Flight Hall Thrusters SPT-70 & SPT-100 After Cathode Change Start During 20-25ms,” *30th International Electric Propulsion Conference*, no. IEPC-2007–062, 2007.

APPENDIX A – CATHODE START-UP PROCEDURE

Table A.1 outlines the time sequenced start-up procedure used to condition and commence cathode operation. This procedure should be used after the chamber has been pumped down and prior to thruster operation. The length of the procedure is based on whether or not the cathode has been exposed to the atmosphere between uses. The cathode insert is porous and is easily contaminated with oxygen and water vapor when exposed to atmospheric conditions. Slowly heating the insert and purging it with propellant gas removes impurities that would cause the cathode to fail during operation. Permanent failure can result if purging is not done properly.

There are three cases outlined in Table A.1. The appropriate case should be selected and followed to condition and start the cathode. The cases are as follows:

Case 1: Used when the cathode has been exposed to the atmosphere for more than a day and the cathode and/or the cathode has not been operated within the last week.

Case 2: Used when the cathode has been operated in the last day but the chamber has been vented. Chamber vent time should not exceed six hours in this case.

Case 3: Used when the cathode has been operated within the last week but has remained under high vacuum since its last operation (chamber has not been vented at all).

Table A.1. Time-Sequenced Start-up Procedure for Cathode.

Heater Current (A)	Minimum Time Required at Each Current Setting (min)		
	Case 1	Case 2	Case 3
2.0	30	10	-
3.0	30	10	-
4.0	5	5	-
5.0	5	5	-
5.5	5	5	-
6.0	5	5	5
6.5 *	5	5	5
7.0	5	5	5
7.5	5	5	5
8.0	5	5	5
*- attempt to start cathode here after minimum time requirement			

To start the cathode conditioning process, set the cathode mass flow to 5 sccm and turn on the cathode heater power supply. Set the power supply to the appropriate current output and increase the current according to the table above. Ensure the heater power supply is in current control mode. After the wait time at 6.5 A is over, turn on the keeper power supply and ensure it is in voltage control mode but set the current limit to ~0.7 A. Energize the keeper by slowly turning up the voltage to a maximum of 150 V. When the cathode “lights” the keeper will draw current (up to the current setting mentioned above) and the voltage will drop to approximately 15 V. If the keeper does not light at first, increase the heater current, wait the appropriate time and try again. Repeat as necessary, but do not exceed a heater current of 8.0 A. Once operational, adjust the keeper current to 0.7 A, the heater current to 6.0 A and the cathode flow rate to 3 sccm. The heater current is reduced to 6.0 A (or less) as temperatures corresponding to heater currents above this will slowly shorten the insert lifetime.

APPENDIX B – SYSTEM WIRING DIAGRAM AND THRUSTER START-UP PROCEDURE

Figure B.1 is the system wiring diagram for the SPT-70 in the HTECh.

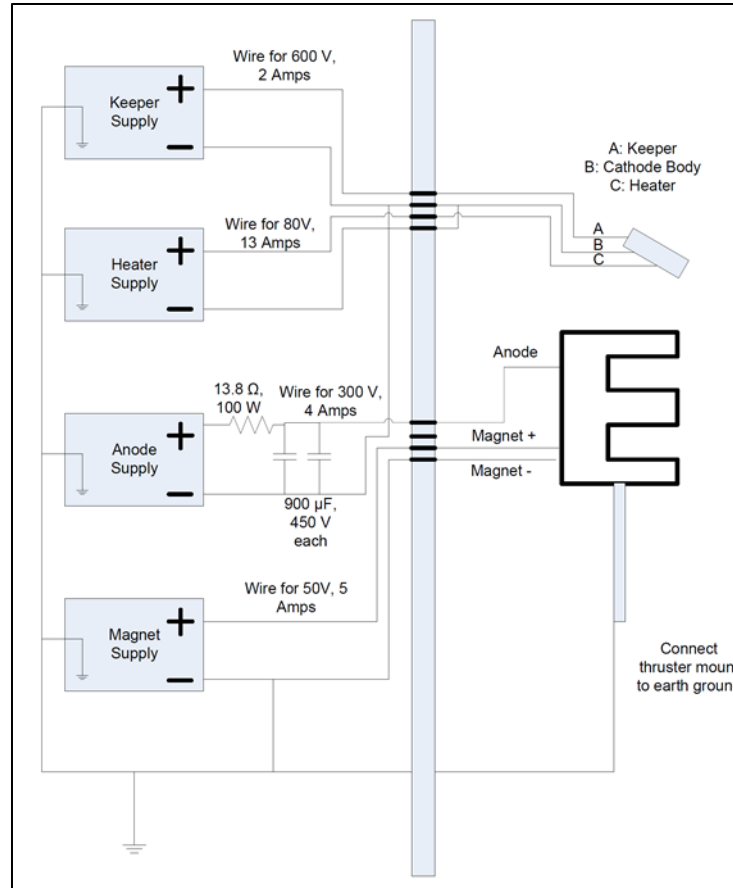


Figure B.1. SPT-70 Wiring Diagram.

The remainder of this appendix outlines the procedure to start and operate the SPT-70 and is used after the cathode is operating. The flow rate of a cathode optimized to the SPT-70 should be between 1 sccm to 3.5 sccm (0.1 mg/s – 0.35 mg/s). Typically the cathode flow rate is set to 10% of the anode flow rate [49]. However, the cathode used in the HTECh is not optimized for an SPT-70. Due to the simple design of the cathode, a higher mass flow rate is needed to produce sufficient electrons for thruster operation. The flow rate to the cathode should be set to 3 sccm. However, the current mass flow controllers on the HTECh are only accurate

down to 5 sccm, so flow rates below that setting are not necessarily accurate. Additionally, it was discovered that the flow through the high purity regulator used with the HTECh oscillates at a low frequency. This oscillation translates to the plasma and can be seen in the plume. The flow oscillation also causes noticeable instabilities in the anode power supply voltage and current settings.

To help with oscillations caused by the regulator on the propellant bottle and overall mass flow accuracy, a small (0.5 L) propellant reservoir is used during thruster operation. The reservoir should be charged to 50 psi using the valves on the propellant lines prior to thruster operation. Ensure the exit valve on the regulator is closed after charging the reservoir. Next, ensure the anode power supply is in voltage control mode with its current limit set to 2.2 A. Set the anode mass flow to 13.5 sccm and increase the anode voltage to around 100 V. Purple colored plasma should be seen at the thruster's exit plane. Next, apply current to magnets until its power supply reaches approximately 2.0 A. Neon-blue colored plasma should now be seen in the thruster's exit plane as trapped electrons in the discharge channel are now ionizing the propellant.

The anode mass flow should be set around 24 sccm, however, as the anode flow rate is increased past 13.5 sccm, the anode voltage will not exceed 90 V. The anode voltage will remain low even as the magnet current is increased above 2 A. This issue may be due to degraded magnetic circuitry.

Table B.1 shows the operating conditions of each of the thruster's supporting components, small variations to these settings are allowable during operation.

Table B.1. Prescribed operating conditions for the SPT-70 in the HTECh.

Component	Operating Condition
Cathode Heater Power Supply*	7.5 V, 6.5 A
Cathode Keeper Power Supply**	14 V, 0.7 A
Cathode Mass Flow Controller	3 - 5 sccm
Thruster Anode Power Supply***	330 V, 2 A
Thruster Magnets Power Supply	5 V, 2 A
Thruster Mass Flow Controller	13.5 – 26 sccm
*- current can be reduced after thruster is operating ** - voltage can be reduced after thruster is operating *** - up to 30V is dropped across the ballast	

Additionally, after the thruster is operating, the heater current should be reduced to zero and the keeper voltage reduced to 5 V and 0.4 A. This step is recommended to prolong the life of the cathode insert. The keeper voltage and current should be monitored to ensure the cathode continues to operate. If the keeper current goes to zero, the cathode will cease and thruster operation will end. In this case, restart the cathode using Case 3 in Appendix A and bring the thruster back into operation. Monitor the anode voltage and current and adjust as needed to meet specified operating conditions.